The 4th YRA MedTech Symposium is jointly organized by the FH Aachen, the University of Duisburg-Essen, the Hochschule Hamm Lippstadt and the Westfälische Hochschule

2024

Symposium Proceedings

Editors:
Ilya Digel (FH Aachen)
Manfred Staat (FH Aachen)
Jürgen Trzewik (Hamm-Lippstadt University of Applied Sciences)
Stefanie Sielemann (Hamm-Lippstadt University of Applied Sciences)
Daniel Erni (University Duisburg Essen)
Waldemar Zylka (Westfälische Hochschule)

YRA – Young Researchers Academy MedTech in NRW

Ph.D., Master, and Bachelor students of all universities in NRW (Uni & FH) working in fields related to biomedical engineering are kindly invited to present their research or their thesis at the

4th YRA MedTech Symposium

February 1 / 2024 / FH Aachen
FH Aachen / Campus Jülich
Heinrich Mußmann Str. 1
52428 Jülich

http://www.yra-medtech.de/

Dear Participants and esteemed Guests,

The field of biomedical engineering has always captivated us with its fascinating challenges, and in recent times, it has evolved into a digital, multidisciplinary domain of significant influence. With great pleasure we announce the resurgence of the Young Researcher Academy (YRA) MedTech Symposia, a platform crafted to provide Ph.D., master, and bachelor students in biomedical engineering with an invaluable space for the exchange of experiences, the presentation of ideas, and the sharing of knowledge.

These symposia have proven to be not only inspiring and instructive but have also fostered direct engagement with experts, offering participants a unique opportunity to interact with experts in the field. Our commitment to nurturing the next generation of biomedical engineers remains steadfast, and we are excited to witness the collective growth that emerges from these collaborative endeavors.

The breadth of research fields covered in the YRA MedTech Symposia is truly expansive, encompassing areas such as biomechanics, implants, microfluidics, bioinformatics, hospital engineering, bioelectronics, biophysics, medical physics, medical imaging, biosensorics, bioanalytics and many more. The diversity of topics reflects the dynamic nature of contemporary biomedical engineering, showcasing the limitless possibilities that lie ahead.

Moreover, this symposium is now increasingly addressing the growing importance of regulatory requirements in medical product development, emphasizing the need for compliance and adherence to evolving standards in this ever-advancing field.

The journey of the YRA Symposium began in Duisburg in 2016, followed by the 2nd YRA MedTech Symposium 2017 as a parallel event alongside the IEEE Workshop/Sensorica in Mühlheim an der Ruhr and the third symposium in 2019 at the Campus Jülich of the Aachen University of Applied Sciences. Unfortunately, the momentum was disrupted by the global challenges posed by the Covid-19 pandemic.

With the **4th YRA MedTech Symposium 2024**, we are delighted to announce the return of this regular event and we extend our heartfelt gratitude to all contributors who have played a vital role in making this resurgence possible. Hello, thank you, and welcome back to this enriching platform that continues to shape the future of biomedical engineering. Your dedication and commitment are the driving forces behind the success of the YRA MedTech Symposia.

Warm regards,

YRA MedTech 2024 Organizing Committee
Prof. Dr. Ilya Digel
Prof. Dr.-Ing. Manfred Staat
Prof. Dr.-Ing. Jürgen Trzewik
Prof. Dr. Stefanie Sielemann
Prof. Dr. Waldemar Zylka
Prof. Dr. sc. techn. Daniel Erni

ISBN 978-3-940402-65-3
DOI: 10.17185/duepublico/81475

Agenda YRA MedTech Symposium 2024

10:00	**ARRIVAL AND REGISTRATION**
11:00	**GREETINGS: Prof. Dr. Ilya Digel (FH Aachen Uiversity of Applied Sciences)** **Prof. Dr. Jürgen Trzewik (Hamm-Lippstadt University of Applied Sciences)**
11:15	**KEYNOTE LECTURE: The EU Medical Device Regulation: Regulation or Overregulation of Market Access?** **Ralf Klein Radimed GmbH, 44805 Bochum**
12:15	**Session I: Regulatory aspects and validation** **Chair: Prof. Dr. Jürgen Trzewik - Hamm-Lippstadt University of Applied Sciences**
12:20	**Navigating innovation within regulatory constraints: The development and authorization journey of fasciotens® Abdomen from product idea to initial patient application** ***Stefan Behle***[1, 2] *Gereon Lill*[1] *and Jürgen Trzewik*[2] [1] *fasciotens GmbH, D-50858 Cologne, Germany* [2] *Hamm-Lippstadt University of Applied Sciences, D-59063 Hamm,Germany*
12:40	**Strategic planning of a usability study for medical devices for the treatment of abdominal wall defects in newborns** ***Jonas Dräger***[1], *Stefan Behle*[2], *Jürgen Trzewik*[1] *and Gereon Lill*[2] [1] *Hamm-Lippstadt University of Applied Sciences, D-59063 Hamm, Germany* [2] *fasciotensGmbH, D-50858Cologne, Germany*
13:00	**Navigating Development and Compliance: Regulatory Requirements for a Patient Positioning System in Breast Cancer Radiotherapy** ***Marvin Christopher Stegmann***[1,2], *Maximilian Even*[1,2], *Sabina Stroh*[1,2], *Hans-Willi Breyer*[1] *and Jürgen Trzewik*[1] [1] *Projekt X-Akt Mamma RTX, Hamm-Lippstadt University of Applied Sciences, D-59063 Hamm, Germany* [2] *GermanPhysics GmbH, Kornkamp 10 a, D-26607 Aurich, Germany*
13:20	**HYBT - A combined radiation technique for breast cancer using the Eclipse™ version 15.6 planning system from Varian Medical Systems** ***Sabina Stroh***[1,2], *Maximilian Even*[1,2], *Raphaela Berghs*[1,2]*and Christopher Stegmann*[1,2] [1] *Projekt X-Akt Mamma RTX, Department Hamm 1, Hamm-Lippstadt University of Applied Sciences, D-59063 Hamm, Germany* [2] *GermanPhysics GmbH, Kornkamp 10 a, D-26607 Aurich, Germany*
13:40	**A software-based Heart Model for Formal Verification and Real-Time Validation of Medical Devices** ***Joseline Heuer***[1], *René Krenz Baath*[1] *and Roman Obermaisser*[2] [1] *Department Hamm 1, Hamm-Lippstadt University of Applied Sciences, D-59063 Hamm, Germany* [2] *Institute for Embedded Systems, University of Siegen, D- 57076 Siegen, Germany*
14:00	**Pause + Poster Session**
14:30	**Session II: Applications** **Chair: Prof. Dr. Ilya Digel - FH Aachen**
14:30	**Gender Differences with Respect to Electromagnetic Power Absorption in Human Skin Tissue at 5G/6G Frequencies** ***Sinan Doğusan***, *Mandana Jalali, Jan Taro Svejda, and Daniel Erni* *General and Theoretical Electrical Engineering (ATE), Faculty of Engineering, University of Duisburg-Essen, and CEDINE – Center for Nano integration Duisburg-Essen, D-47058 Duisburg, Germany*
14:50	**Assessment of Temperature Changes caused by 7T MRI Scans using Proton Resonance Shift Thermometry** ***Maíra Martins Garcia***[1,2], *Daniel Erni*[2] *and Waldemar Zylka*[1] [1] *Faculty of Electrical Engineering and Applied Natural Sciences, Westphalian University, D-45897 Gelsenkirchen, Germany* [2] *General and Theoretical Electrical Engineering (ATE), University of Duisburg-Essen, and CENIDE – Center of Nanointegration Duisburg-Essen, D-47048 Duisburg, Germany.*
15:10	**Vat Photopolymerization 3D Printing on Glass Substrates for the Fabrication of Microfluidic Systems** ***Frederik Morgenroth***, *Benedikt Emde and Lara Tickenbrock* *Hamm-Lippstadt University of Applied Sciences, D-59063 Hamm*

15:30	**Non invasive analysis of hospital acquired pneumonia by ion mobility mass spectrometry in parallel** ***Hannah Schanzmann***[1,2,3], *Parviz Ahmad-Nejad*[2], *Veronika Ruzsanyi*[4], *Ursula Telgheder*[3] *and Stefanie Sielemann*[1] [1] *Laboratory of Applied Instrumental Analytical Chemistry, Hamm-Lippstadt University of Applied Sciences, 59063 Hamm, Germany* [2] *Institute for Medical Laboratory Diagnostics, Helios University Clinic Wuppertal with Witten/Herdecke University, 42283 Wuppertal/ 58455 Witten, Germany* [3] *Department of Instrumental Analytical Chemistry, University of Duisburg-Essen, 45141 Essen, Germany* [4] *Institute for Breath Research, University of Innsbruck, 6020 Innsbruck, Austria*
15:50	**Magnetic biosensing with magnetic nanoparticles: Simulative approach to predict signal intensity in frequency mixing magnetic detection** ***Beril Simsek***[1], *Hans-Joachim Krause*[1,2] *and Ulrich M. Engelmann*[1] [1] *Medical Engineering and Applied Mathematics, University of Applied Sciences Aachen, D-52428 Jülich, Germany* [2] *Institute of Biological Information Processing, Bioelectronics (IBI-3), Forschungszentrum Jülich, D-52428 Jülich, Germany*
16:10	**Effect of different cannula positions in the pulmonary artery on blood flow and gas exchange using computational fluid dynamics analysis** ***Annika Schmitz***[1], *Shah Eiman Amzar Shah Apandi*[1], *Jan Spillner*[2], *Flutura Hima*[2] *and Mehdi Behbahani*[1] [1] *Institute for Bioengineering (IfB), Faculty for Medical Engineering and Techno-Mathematics, University of Applied Sciences Aachen, D - 52428 Jülich, Germany* [2] *Department of Thoracic and Cardiovascular Surgery, Medical Faculty, University Hospital RWTH Aachen, 52074 Aachen, Germany*
16:30	**EEM spectroscopy characterization of humic substances of biomedical importance** ***Dinara Sherelkhan***[1,2] *and Alina Alibekova*[1] [1] *Institute of Ecological Problems, Al-Farabi Kazakh National University, Almaty 050040, Kazakhstan* [2] *Institute for Bioengineering (IfB), Faculty for Medical Engineering and Techno-Mathematics, University of Applied Sciences Aachen, D - 52428 Jülich, Germany*
16:50	**AstroBioLab: Review of Technical and Bioanalytical Approaches** ***Atakan Tepecik*** *Institute for Bioengineering (IfB), Faculty for Medical Engineering and Techno-Mathematics, University of Applied Sciences Aachen, D - 52428 Jülich, Germany*
17:10	**Summary and concluding discussion**
17:30	**End**
	POSTER SESSION PARTICIPANTS:
Stand 1	**On-site treatment of hospital wastewater in a full-scale treatment plant in Germany: Evaluation of treatment performance** ***Sarah Häußer***[1,2], *Martin Weber*[4], *Christian Mauer*[5], *Volker Linnemann*[3], *Anna Pfannstiel*[2], *Johannes Pinnekamp*[3], *Thomas Wintgens*[3], *Claudia Klümper*[1] *and Silvio Beier*[2] [1] *Department Hamm 2, Hamm-Lippstadt University of Applied Sciences, D-59063 Hamm, Germany* [2] *Bauhaus-Institute for infrastructure solutions (b.is), Bauhaus-Universität Weimar, D-99423 Weimar, Germany* [3] *Institute of Environmental Engineering, RWTH Aachen University, D-52074 Aachen, Germany* [4] *Aggerverband, D-51645 Gummersbach, Germany* [5] *Weber-Ingenieure GmbH, D-75177 Pforzheim, Germany*
Stand 2	**Development of a breast phantom to validate a novel patient positioning system for breast cancer radiotherapy** ***Ganna Papakina***[1], *Frederik Morgenroth*[1], *Jürgen Trzewik*[1] *and Marvin Christopher Stegmann*[1,2] [1] *Hamm-Lippstadt University of Applied Sciences, D-59063 Hamm, Germany* [2] *GermanPhysics GmbH, Kornkamp 10 a, D-26607 Aurich, Germany*

Stand 3	**Noise Signals and Simulation Analysis of Front-End Amplification Circuit in Silicon Photomultipliers (SiPM) Radiation Detectors Based on Positron Emission Tomography (PET)** ***Chengxi Hua***[1], *Hans-Josef Ackermann*[2] *and Karl Ziemons*[1] [1] *Laboratory of Medical Physics, Faculty of Medical Engineering and Technomathmatics, University of Applied Sciences Aachen, D - 52428 Jülich, Germany;* [2] *Faculty of Medical Engineering and Technomathmatics, Aachen University of Applied Sciences, D-52428 Jülich, Germany*
Stand 4	**AstroBioLab: Review of Technical and Bioanalytical Approaches** ***Atakan Tepecik*** *Institute for Bioengineering (IfB), Faculty for Medical Engineering and Techno-Mathematics, University of Applied Sciences Aachen, D - 52428 Jülich, Germany*
Stand 5	…

Keynote Lecture

Will the new European Medical Device Regulation 2017/745 really lead to better and, above all, safer medical devices? Or is it an over-regulation?

Ralf Klein[(1)]
[(1)] Radimed GmbH, D-44805 Bochum, Germany

Abstract – 7 years of experience with the new regulation show a clear bottleneck in supply due to discontinued products. Extremely increased costs and bureaucratic effort on the part of both manufacturers and notified bodies contrast with a supposed improvement in safety.

What was the trigger to restructure market access in Europe in this way and were medical devices really so unsafe and dangerous "in the past"?

The presentation will give a brief overview of the history of market access for medical devices on the European market, show the current state of affairs using examples from the market and - if at all possible - give an outlook on what is yet to come.

Session I: Regulatory aspects and validation

Navigating innovation within regulatory constraints: The development and authorization journey of fasciotens®Abdomen from product idea to initial patient application

Stefan Behle[1/2], Gereon Lill [1] and Jürgen Trzewik[2]

[1] fasciotens GmbH, D-50858 Cologne, Germany

[2] University of Applied Sciences Hamm-Lippstadt, D-59063 Hamm, Germany

E-Mail: behle@fasciotens.de

Abstract

The objective of this study was the development and implementation of a registration strategy for innovative medical devices, exemplified by the journey of fasciotens®Abdomen from conceptualization to its initial application on patients.

More than half of all ideas for new medical products come from the practical work of healthcare professionals. The idea of fasciotens®Abdomen is no exception [patent no. LIL0001-WO.EP]. The product fasciotens®Abdomen was developed out of a medical need for the treatment of open abdomens. An open abdomen or laparostomy may be necessary for survival as a result of injuries, abdominal infections or complications following abdominal surgery [1]. The treatment of an open abdomen is challenging and the mortality rate is reported to be 12-40 % [2]. The abdominal wall fascia retracts due to the lack of tension at the edges of the open abdominal wall. Subsequent closure of the abdominal wall is difficult or even impossible and can lead to large abdominal wall hernias with considerable consequential problems and frequent repeat operations. The treatment with fasciotens®Abdomen applies tension to the open abdominal wall and is intended to counteract its regression.

Three success criteria were defined for this study. The first criterion to be fulfilled was the CE conformity and certification of the product according to Annex V and VII of Directive 93/42/EEC [3]. Secondly, the certification of the quality management system and thus the proof of conformity with DIN EN ISO 13485:2016 should be achieved [4]. The final third success criterion was the successful product implementation in the market and the resulting first product application on patients.

To achieve the defined success criteria, a strategy path was defined by the German Federal Association for Medical Technology based on the five phases of a medical product described above and depending on the risk class of the medical product following the Medical Device Directive (MDD) (93/42/EEC). The implementation of the strategy path was based on the concrete example of fasciotens®Abdomen. The development of the product was accompanied and documented. Furthermore, technical documentation was established for the product according to the requirements of the MDD. Additionally, the development of a quality management system (QMS) according to DIN EN ISO 13485 was accompanied and established for the company. With the successful certification of the product and the QMS by a notified body, the first two success criteria were achieved. The following market launch of the product and the promising therapeutic successes confirmed the rewards of many years of development. The third success criterion of this thesis was also achieved.

Since its market launch in 2019, the product has been established and used extensively in the surgical field. Due to regulatory changes, the product is currently undergoing the MDR approval process together with two other developed products [5]. An overview of the current certification process will be provided as an outlook.

References

[1] Li, X. et al. Open abdomen treatment for complicated intra-abdominal infection patients with gastrointestinal fistula can reduce the mortality. Medicine 99, e19692 (2020).

[2] Bruhin, A., Ferreira, F., Chariker, M., Smith, J. & Runkel, N. Systematic review and evidence based recommendations for the use of negative pressure wound therapy in the open abdomen. Int J Surg 12, 1105-1114 (2014).

[3] Council Directive 93/42/EEC of 14 June 1993 concerning medical devices

[4] ISO 13485:2016 - Medical devices -- Quality management systems -- Requirements for regulatory purposes".

[5] Regulation (EU) 2017/745 of the European Parliament and of the Council of 5 April 2017 on medical devices, amending Directive 2001/83/EC, Regulation (EC) No 178/2002 and Regulation (EC) No 1223/2009 and repealing Council Directives 90/385/EEC and 93/42/EEC (Text with EEA relevance.

Strategic planning of a usability study for medical devices for the treatment of abdominal wall defects in newborns

Jonas Dräger[(1)], Stefan Behle[(2)], Jürgen Trzewik[(1)] and Gereon Lill[(2)]

[(1)] University of Applied Sciences Hamm-Lippstadt, D-59063 Hamm, Germany
[(2)] fasciotens GmbH,
D-50858 Cologne, Germany
E-Mail: jonas.draeger@stud.hshl.de

Abstract
The objective of this work is the strategic development of a study design focusing on the usability of medical devices for the treatment of abdominal wall defects in newborns. The strategic planning of the usability study serves as a foundation for evaluating whether a usability test needs to be carried out.

The advancement of medical technology has led to a widespread use of medical devices in various areas of medicine. The growing number of such products used by healthcare professionals and patients has led to new requirements, particularly in terms of safety and usability. [1] Manufacturers are legally obligated to demonstrate compliance with essential safety and performance requirements according to standards such as IEC 62366 and MDR to ensure the medical benefits of their devices. [2, 3]

To meet these requirements, we closely examined the regulatory requirements of MDR and IEC 62366. This enabled the creation of a usability engineering file for the devices containing the use specifications, use-related-risk analysis and user specifications. The use specifications contain detailed information about the use of the medical devices, their users and their tasks. The userelated-risk analysis examines potential risks during product usage and the effects on the user and patient. The user interface specifications describe the user interfaces and their specific requirements. In addition, a guideline was created for a possible summative usability test, derived from the results of the specifications and the hazardous risks of the use-related risk analysis. The test consists of five cases, designed to be conducted by user groups consisting of pediatric surgeons and nurses.

Following an analysis comparing devices of the product family and the created engineering files, a rationale was established which made the need for a usability test obsolete. Consequently, the evaluation of the product usability has been completed and further tests are considered unnecessary.

References

[1] C. Backhaus, "Entwicklung einer Methodik zur Analyse und Bewertung der Gebrauchstauglichkeit von Medizintechnik: PROMEDIKS – Prozessorientierte Medizintechnik in klinischen Systemen," Dissertation, TU Berlin, Berlin, 2004.
[2] Europäisches Parlament und Rat der Europäischen Union, "MDR (EU) 2017/745," *Amtsblatt der Europäischen Union*, 2017.
[3] *Medical devices — Part 1: Application of usability engineering to medical devices*, IEC 623661:2015, International Electrotechnical Commission, Feb. 2015.

Navigating Development and Compliance: Regulatory Requirements for a Novel Patient Positioning System in Breast Cancer Radiotherapy

Marvin Christopher Stegmann[(1/2)], Maximilian Even[(1/2)], Sabina Stroh[(1/2)] ,Hans-Willi Breyer[(1)] and Jürgen Trzewik[(1)]

[(1)]Projekt X-Akt Mamma RTX
Hochschule Hamm-Lippstadt University of Applied Sciences
D-59063 Hamm, Germany

[(2)]GermanPhysics GmbH
Kornkamp 10 a
D-26607 Aurich, Germany
E-mail: c.stegmann@germanphysics.de

Abstract
The goal of this work is to develop a new type of patient positioning system for breast cancer radiotherapy. Adjusting the patient's position on the radiation table aims to enhance the efficiency of radiation treatment, minimizing side effects and improving long-term survival. This is particularly important for breast cancer radiotherapy, as this is the most common cancer in women [1]. Typically, the patient lies on her back with her arms folded at a 90° angle next to or above her head, a critical aspect for reproducibility during fractionated radiation treatment [2]. The side effects of the therapy are known and occur in the surrounding tissue to the radiation region [2] [3]. Special attention should be paid to the heart [4]. By adopting a prone position, a greater distance from the target volume to organs at risk is achieved, minimizing the risk of late complications. (see Figure 1).

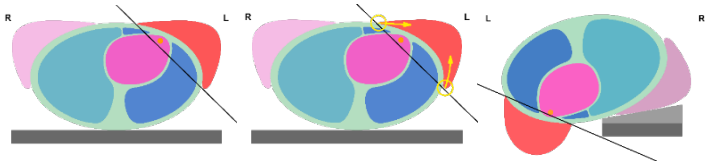

Fig. 1: Patient in supine position, radiation fields cut through the heart. (left fig.) / the breast wraps around the thorax in supine position (middle fig.) / patient in prone position, the breast automatically falls away from the organs at risk due to gravity (right fig.)

The envisioned system should be able to be attached to existing radiation tables from common manufacturers. The aim was to find out the regulatory requirements for a patient positioning system in radiotherapy before starting the project. The medical purpose of the product is to improve an established therapy on the market. Requirements for the positioning system were compiled from three main areas: product requirements, product environment requirements, and regulatory requirements as summarized in Figure 2. The assignment of the system to a medical device class further defined the required framework [5], and according to classification application rules, our system was categorized as class I.
The first area, product requirements, resulted in more general requirements, primarily focusing on the main features of the product. Considerations was given to patents, competitor products and their advantages and disadvantages. Independent customer requirements analysis supplemented the company's product considerations, aiding in product planning and creating a unique selling point. The product environment provides insights about users, patients, and the medical environment. The third area of requirements deals with regulatory requirements; the applicable laws and guidelines are considered here. The Medical Device Regulation (MDR) applies to medical devices with the aim of increasing the quality and safety of medical devices [5]. Reference is made to various system standards which are applicable to all medical devices and which must be consulted during implementation. The requirements must be supplemented by the product standards applicable to the

product itself. A standards search must be carried out for this purpose. In the case of a niche product such as the positioning system, where direct product standards may be lacking, the standards for similar products or those with a similar product environment must also be taken into account here.

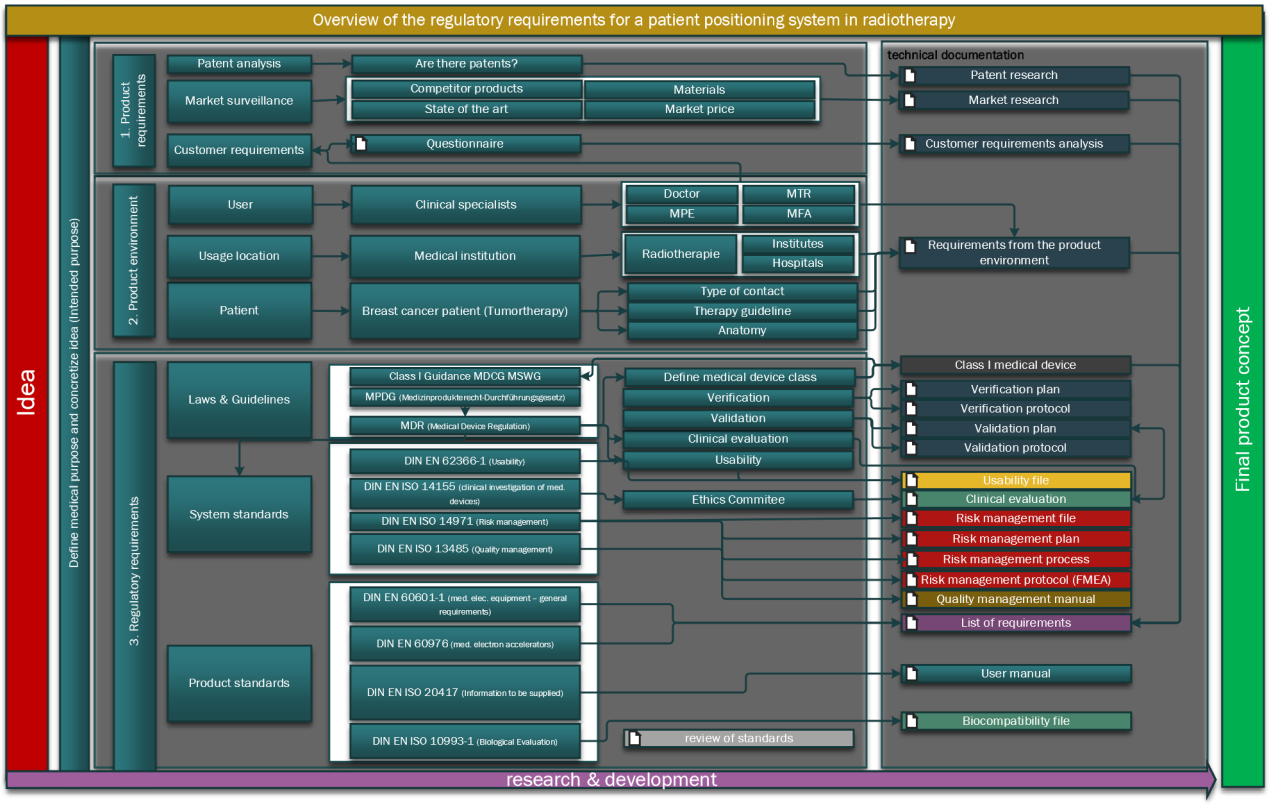

Fig. 2: Overview of the requirements for a patient positioning system in radiotherapy

All requirements were consolidated in a list of requirements, detailing the origin, planned implementation and final execution. To facilitate medical device certification, the entire technical documentation from the start of development to the finished product, including the implementation of regulatory requirements, must be clear to an auditor. A review of standards was created for this purpose, containing all regulatory requirements with corresponding references to the documents in which the implementation is documented.
Exclusions were justified, enabling a precise audit trail of each point's implementation. In summary, developing a medical device, even for a Class I medical device, demands careful consideration of requirements from various areas to ensure product safety.

References

[1] R. Koch-Institut, *Krebs in Deutschland | 2015/2016*, doi: 10.25646/5977.2.

[2] M. Wannenmacher, F. Wenz, und J. Debus, Eds., *Strahlentherapie*. Berlin, Heidelberg: Springer, 2013. doi: 10.1007/978-3-540-88305-0.

[3] "Leitlinienprogramm Onkologie (Deutsche Krebsgesellschaft, Deutsche Krebshilfe, AWMF): S3-Leitlinie Früherkennung, Diagnose, Therapie und Nachsorge des Mammakarzinoms, Version 4.3, 2020, AWMF Registernummer: 032-045OL, http://www.leitlinienprogramm-onkologie.de/leitlinien/mammakarzinom/“, 2020.

[4] M. D. Piroth *u. a.*, "Heart toxicity from breast cancer radiotherapy: Current findings, assessment, and prevention“, *Strahlenther Onkol*, vol.. 195, no. 1, pp. 1–12, Jan. 2019, doi: 10.1007/s00066-018-1378-z.

[5] "Verordnung (EU) 2017/745 des Europäischen Parlaments und des Rates - vom 5. April 2017 - über Medizinprodukte, zur Änderung der Richtlinie 2001/ 83/ EG, der Verordnung (EG) Nr. 178/ 2002 und der Verordnung (EG) Nr. 1223/ 2009 und zur Aufhebung der Richtlinien 90/ 385/ EWG und 93/ 42/ EWG des Rates“.

HYBT - A combined radiation technique for breast cancer using the Eclipse™ version 15.6 planning system from Varian Medical Systems

Sabina Stroh[(1)(2)], Maximilian Even[(1)(2)], Raphaela Berghs[(1)(2)], Jürgen Trzewik[(1)], Christopher Stegmann[(1)(2)]

[(1)] Projekt X-Akt Mamma RTX
Hochschule Hamm-Lippstadt University of Applied Sciences
D-59063 Hamm, Germany

[(2)] GermanPhysics GmbH
Kornkamp 10 a
D-26607 Aurich, Germany
E-mail: s.stroh@germanphysics.de

Abstract – Breast cancer radiotherapy requires individualized planning and can be delivered using a variety of radiotherapy techniques, which have evolved over the years. These include Three-Dimensional Conformal Radiation Therapy (3DCRT), Intensity Modulated Radiation Therapy (IMRT) and Volume Modulated Arc Therapy (VMAT). All techniques are still used today and have advantages and disadvantages.

The aim of this work is to combine the advantages of 3DCRT and VMAT to create a hybrid planning of 3DCRT and VMAT (HYBT) in relation to breast irradiation.

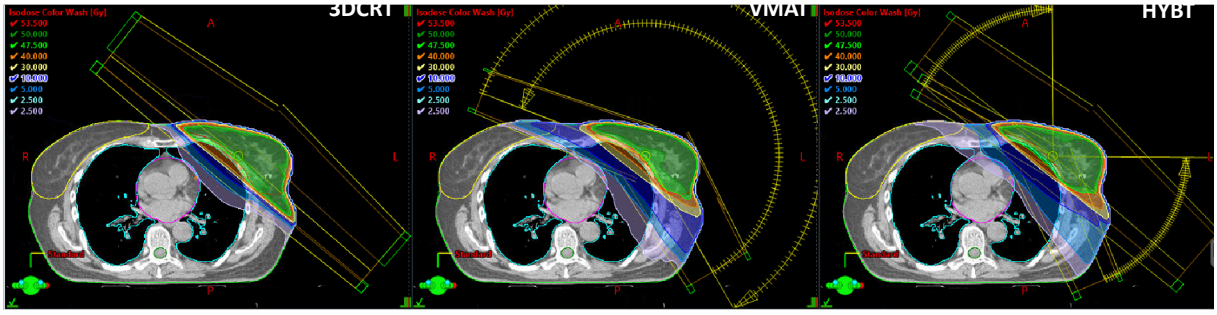

Fig. 1: Transversal views of treatment plans in 3D Conformal Radia;on Therapy (3DCRT), Volume Modulated Arc Therapy (VMAT) and hybrid plan of 3DCRT and VMAT (HYBT)

Figure 1 shows the different techniques next to each other with the isodose distribution. 3DCRT uses four to eight static fields to homogenize the dose in the target volume [1]. The beams are applied from only two directions to create a tangent. VMAT is using more directions of radiation and smaller fields to optimize the prescribed dose in the target volume. As a combined technique HYBT applies approx. 80 % of the prescribed dose with the tangential technique and uses two arcs to saturate the remaining dose.

The advantages of 3DCRT and VMAT were combined and converted into an HYBT. A plan was created for planning with a prescription of 50 Gy with 25 fractions. According to ICRU Report 50, irradiation plans should cover the entire PTV at 95% dose and should not reach a dose higher than 107%, so the plans are based on these values [2]. The two beam directions of the 3DCRT were used. The static fields were applied with an anterior safety margin of three centimeters. Afterwards the

beams were renormalized to 80% of the prescribed dose so that the remaining dose could be saturated with two arcs of approx. 60°- 90°. The same isocenter was used for the supplementary VMAT planning as for 3DCRT, so that an entire plan could then be combined from two individual plans. The beam angles were designed so that they don't radiate frontally through the heart. The collimator was tilted by ten degrees so that the lead aperture and the multi-leaves could be adjusted to the trailing edge of the target volume. In the optimization step, 3DCRT was added as a base dose plan and the dose to the organs at risk was optimized. After the calculation, the static fields with the corresponding MU were copied into VMAT plan and calculated as one plan.

The result shows that there is a possibility of combining 3DCRT and VMAT. The primary dose is applied by the two static fields to achieve the effect of the tangential beams. The dose saturation by using VMAT simplifies the planning of complex target volumes. VMAT alone uses more MU due to the multiple directions of radiation. HYBT can lower the MU numbers in comparison to VMAT alone. The isodose distribution of 3DCRT is smaller in the low-dose range considering the distant organs. Considering the 95% of the prescribed dose there is more dose in the normal tissue compared to VMAT. Among these advantages HYBT combines the conformity of the isodose distribution.

There is a safety space in the anterior direction of the patient to assure the radiation during respiration by using 3DCRT or HYBT. VMAT doesn't have a safety space. This technique is only recommended by using some respiratory tracking to verify the radiation while moving. Furthermore, 3DCRT has the lower MU numbers. The more optimization of small fields and radiation directions are used, the higher the MU. Rotational irradiations lead to more scattered radiation in more distant organs, which can induce a secondary carcinoma [3].
The isodose distribution of VMAT has advantages and disadvantages compared to 3DCRT. The high-dose areas in normal tissue outside the target volume can be reduced, while larger areas of the body receive a lower dose. This is due to the larger number of beam directions and the increased number of monitor units, which in turn leads to increased scattered radiation from the accelerator head [4].
Even the guidelines for breast cancer recommend VMAT only for patients with larger breasts or abnormal thoracic curvature (e.g. funnel chest) [5].

However, HYBT can be a compromise for planning complex target volumes, where the primary dose comes from two 3DCRT-fields combined with the remaining dose optimized by VMAT.

References

[1] H. Sack, N. Thesren, and M. Hillscher, *Bestrahlungsplanung*. Stuttgart: Thieme, 1993.

[2] D. Jones, "ICRU report 50-prescribing, recording and reporting photon beam therapy", *Med. Phys.*, vol 21, no. 6, pp. 833–834, June 1994, doi: 10.1118/1.597396.

[3] E. J. Hall and C.-S. Wuu, "Radiation-induced second cancers: the impact of 3D-CRT and IMRT", *International Journal of Radiation Oncology*Biology*Physics*, vol. 56, no. 1, pp. 83–88, Mai 2003, doi: 10.1016/S03603016(03)00073-7.

[4] M. Wannenmacher, F. Wenz, and J. Debus, (Eds.)., *Strahlentherapie*. Berlin, Heidelberg: Springer Berlin Heidelberg, 2013. doi: 10.1007/978-3-540-88305-0.

[5] Leitlinienprogramm Onkologie (Deutsche Krebsgesellschaft, Deutsche Krebshilfe, AWMF), „S3-Leitlinie Früherkennung, Diagnose, Therapie und Nachsorge des Mammakarzinoms, Version 4.4, 2021, AWMF Registernummer: 032-045OLS3-Leitlinie Mammakarzinom". 2021. Zugegriffen: 16. November 2023. [Online].

http://www.leitlinienprogramm-onkologie.de/leitlinien/mammakarzinom/.

A software-based Heart Model for Formal Verification and Real-Time Validation of Medical Devices

Joseline Heuer[1], René Krenz-Baath[1], and Roman Obermaisser[2]

[1] Department Hamm 1, Hochschule Hamm-Lippstadt, D-59063 Hamm, Germany

[2] Institute for Embedded Systems, University of Siegen,
D- 57076 Siegen, Germany
E-Mail: joseline.heuer@hshl.de
Web: https://www.hshl.de/

Abstract It is crucial to comprehensively verify and validate increasingly complex medical devices to ensure their functional correctness, even in unusual circumstances. Current software-based models of the human heart designed for pacemaker safety verification and validation do not include the chamber or valve status. This constraint reduces the range of test scenarios feasible for the model, since such a model cannot evaluate the variable durations of the vulnerable phase and the chamber coordination that are required to identify life-threatening scenarios. Our model represents the electrical conduction system of the heart, alongside the chambers and ventricles, as distinct modules. The system model has been implemented as a formal verification [1] model and as a hardware-in-the-loop model that is capable of real-time operations. The interaction of the model with a commercially available pacemaker allowed us to demonstrate the occurrence of a malfunction of the pacemaker: the pacemaker syndrome shown in Figure 1.

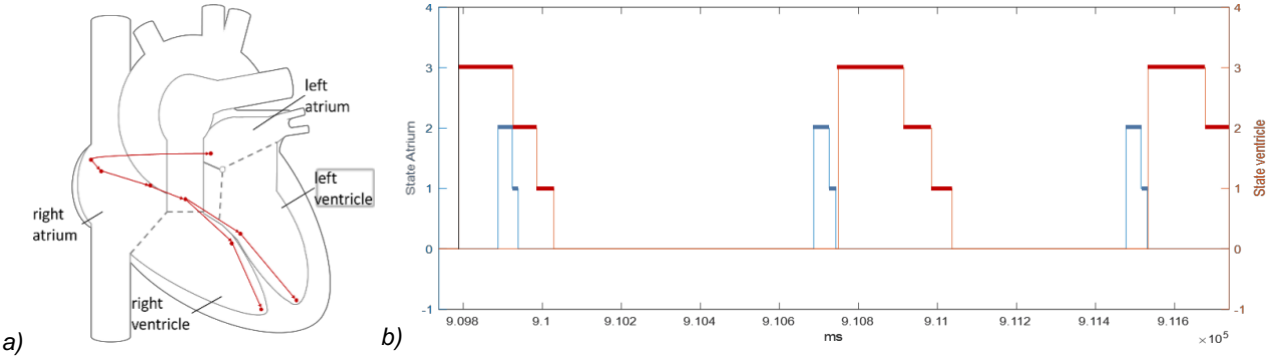

Fig.1: a) Sketch of the Human heart showing the four chambers, in red the electrical conduction system of the heart. b) Interaction of the HIL model with a real pacemaker illustrating the change in state over time in interaction with a pacemaker, marked as black line. The states of the right atrium are shown in blue and state of the right ventricle in red.

Electrical medical implants can vastly enhance a patient's quality of life, or in some cases, even save their lives. However, any malfunction in the operation of these devices can lead to serious and even fatal consequences for the patient. With the systems becoming increasingly intricate in order to cater to individual patient needs, it is crucial to establish a validation and verification framework that aligns with medical regulations, while ensuring comprehensive verification and validation of the system. Pacemakers, surgically implanted in people for years or decades, are an example for such medical devices. It is imperative for the pacemaker to continuously adapt to the changing electrical resistances and frequencies required for the patient's well-being and survival.
The current approval process does not require new algorithms for pacemakers to be evaluated against biological models. In state-of-the-art hardware-in-the-loop (HIL) testing of pacemakers, heart models do not consider the chamber and valve states, see [2]–[5]. This omission prevents adequate consideration of diseases such as the pacemaker syndrome and the onset of a stimulation in vulnerable phases, which may result in ventricular fibrillation, with potentially dramatic implications for the patient. Our model presents the heart as a modular system, consisting of separate timed

automata, functioning simultaneously and communicating via asynchronous channels. The model uses eleven parallel timed automata with individual parameters to describe the operation of the electrical conduction system of the heart. Four additional parallel timed automata with individual parameters are used to describe the chambers. Their interplay is sketched in Figure 1a. The state of each of the four heart chambers undergoes continuous alteration by a single automaton per chamber. State changes rely on individual chamber parameters, as well as the continuously changing stimulation intervals and the recalculated action potential durations. The simulation is based the data of Ref. [6].

Our HIL model allows for the testing of pacemakers available commercially in order to assess their performance in extraordinary circumstances and to enhance and evaluate our verification model. The model can be used to detect faults in the interaction between the heart model and a pacemaker precisely by calculating the vulnerable phase and the state of the valves as a function of the current action potential duration. This enables accurate identification and recording of errors arising from the interaction between the heart and a pacemaker. Examples include stimulation during the vulnerable phase of a ventricle, which may lead to ventricular fibrillation and the occurrence of the pacemaker syndrome resulting in inefficient heart pumping. Furthermore, it is possible to examine and visualize the impact of different malfunctions within the heart's electrical conduction system, with or without the effects of a pacemaker.

For illustration of the model performance we show the collected data for the interaction of the HIL model with a real pacemaker in Figure 1b. For the right atrium (blue) 2 indicates the state, during which the atrium is contracted and cannot be stimulated. State 1 indicates a status in which it starts to relax and can be stimulated, however, a stimulation could lead to arrhythmia – the vulnerable phase. State 0 indicates that the atrium is at rest waiting for a stimulation. For the right ventricle (red) the phase, in which it cannot be stimulated, is labeled as state 3 and state 2 indicates the vulnerable phase. In state 1 the ventricle is further relaxed and can be stimulated without danger, but has not relaxed enough to open the valve between the upper and lower ventricles. Finally, status 0 denotes full relaxation of the ventricle. On the left, a stimulation from the pacemaker is shown as a black line, which triggers the ventricle. It is seen that the stimulation of the ventricle at this point results in a parallel contraction of atrium and ventricle – as the atrium and ventricle are in their contraction state in parallel. This leads to a contraction of the atrium pumping the blood against the closed valve and back into the vein instead of into the ventricle – the pacemaker syndrome. This occurs when the pacemaker does not correctly sense the heart's activity, because it is in an interference mode due to interfering signals, has been inadequately programmed, or is in its energy-saving mode due to low battery power.

The example demonstrates the capability of our HIL model to simulate the heart in a manner that permits testing for critical scenarios, including the pacemaker syndrome as observed in heart-pacemaker interactions. This enables analyses of the interaction between the medical device and the human heart in various circumstances, eventually improving the safety of the patients.

References

[1] J. Heuer, R. Krenz-Bååth, und R. Obermaisser, „Verifying Bio-Electronic Systems“, in *2023 26th International Symposium on Design and Diagnostics of Electronic Circuits and Systems (DDECS)*, Tallinn, Estonia: IEEE, Mai 2023, S. 161–166. doi: 10.1109/DDECS57882.2023.10139574.

[2] E. Yip *u. a.*, „Towards the Emulation of the Cardiac Conduction System for Pacemaker Validation“, *ACM Trans. Cyber-Phys. Syst.*, Bd. 2, Nr. 4, S. 1–26, Okt. 2018, doi: 10.1145/3134845.

[3] C. Barker, M. Kwiatkowska, A. Mereacre, N. Paoletti, und A. Patane, „Hardware-in-the-loop simulation and energy optimization of cardiac pacemakers“, in *2015 37th Annual International Conference of the IEEE Engineering in Medicine and Biology Society (EMBC)*, Milan: IEEE, Aug. 2015, S. 7188–7191. doi: 10.1109/EMBC.2015.7320050.

[4] C. D. Mascio und G. Gruosso, „Hardware in the Loop Implementation of the Oscillator-based Heart Model: A Framework for Testing Medical Devices“, *Electronics*, Bd. 9, Nr. 4, S. 571, März 2020, doi: 10.3390/electronics9040571.

[5] M. Soo Kim, W. Ai, P. S. Roop, N. Allen, R. Ramchandra, und J. Paton, „Formal Modeling and Verification of Rate Adaptive Pacemakers for Heart Failure“, in *2020 18th ACM-IEEE International Conference on Formal Methods and Models for System Design (MEMOCODE)*, Jaipur, India: IEEE, Dez. 2020, S. 1–11. doi: 10.1109/MEMOCODE51338.2020.9315160.

[6] M. R. Franz, C. D. Swerdlow, L. B. Liem, und J. Schaefer, „Cycle length dependence of human action potential duration in vivo. Effects of single extrastimuli, sudden sustained rate acceleration and deceleration, and different steady-state frequencies.“, *J. Clin. Invest.*, Bd. 82, Nr. 3, S. 972–979, Sep. 1988, doi: 10.1172/JCI113706.

Session II: Applications

Gender Differences with Respect to Electromagnetic Power Absorption in Human Skin Tissue at 5G/6G Frequencies

Sinan Doğusan, Mandana Jalali, Jan Taro Svejda, and Daniel Erni

General and Theoretical Electrical Engineering (ATE), Faculty of Engineering, University of Duisburg-Essen, and CEDINE – Center for Nano integration Duisburg-Essen,
D-47058 Duisburg, Germany
E-Mail: sinan.dogusan@uni-due.de
Web: https://www.uni-due.de/ate/

Abstract – In recent years, the need for technical applications with faster and more reliable data transfer has placed the 5G/6G frequency band at the center of scientific research. Consequently, the possible impacts of increased exposure to millimeter wave (mmWave) radiation on human health are causing growing concern. Thus, taking into account the biological properties of the skin tissues, research and comprehension of the effects of such physical exposure on human skin are necessary. It is shown that the epidermis and dermis tissue layers that make up the skin -the largest organ in the human body [1]- have different thickness in each gender [2], and as a result, the skin of each gender will react differently to exposure to electromagnetic (EM) radiation. In this study, human skin was homogeneously modeled in six different body parts (abdomen, back, breast, dorsum of foot, dorsum of hand, and scalp) of male and female individuals of a human population of the same ethnicity in four layers as shown in Fig.1. The gender effect in the corresponding integrated absorbed power and penetration depths was examined using simulation results from the exposure of the twelve human skin models described above to integrated EM waves in the 5G/6G frequency ranges.

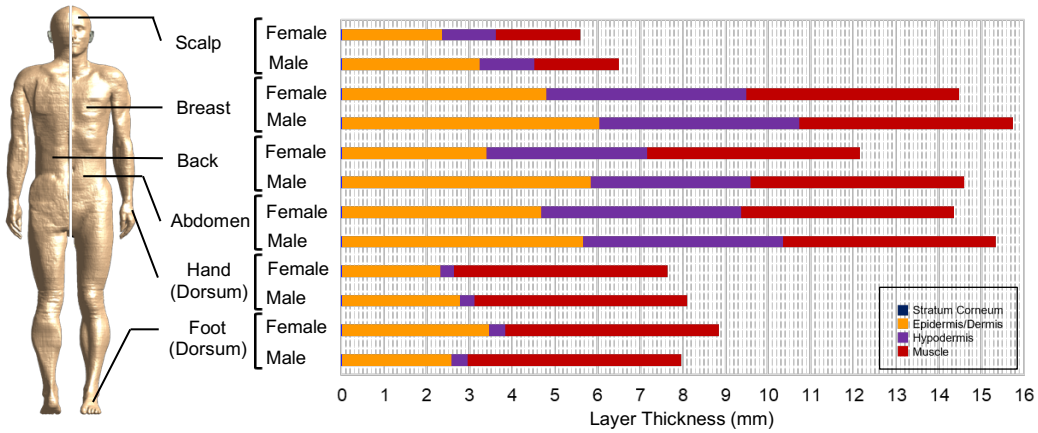

Fig.1: The skin thickness for both genders [2-5]*. The phantom taken from ©Sim4Life* [6].

Result: According to the results of the simulations, gender-based differences in power absorption were identified in four different tissue layers in six different anatomical regions at frequencies between 3-25 GHz. The stratum corneum (the outermost layer of the skin) has minimal power absorption capacity due to its low conductivity, water content and thickness, with gender differences in absorption being negligible. Gender-specific differences were especially prominent in the epidermis/dermis, where the absorbed power was highest. Particularly, in the back region, where there is the most significant difference in epidermis/dermis thickness between genders (males' backs 2.42 mm thicker), gender-based the power absorption difference reached a maximum at 4.8 GHz, and higher absorption was observed on males' backs than females'. In the hypodermis, which is lie under the epidermis/dermis, the absorbed power in six different body regions of female samples were higher than in the same layer of male samples. The foot (dorsum), where males' skin is 26% thinner female skin, was the only body site in which the absorbed power in muscle tissue was higher in females' than in males'. The penetration depth of the electric field (the distance within the body where the electric field strength decreases to 1/e times the initial value at the skin boundary) were calculated for twelve skin models. It is worth noting that gender-based differences were also obvious

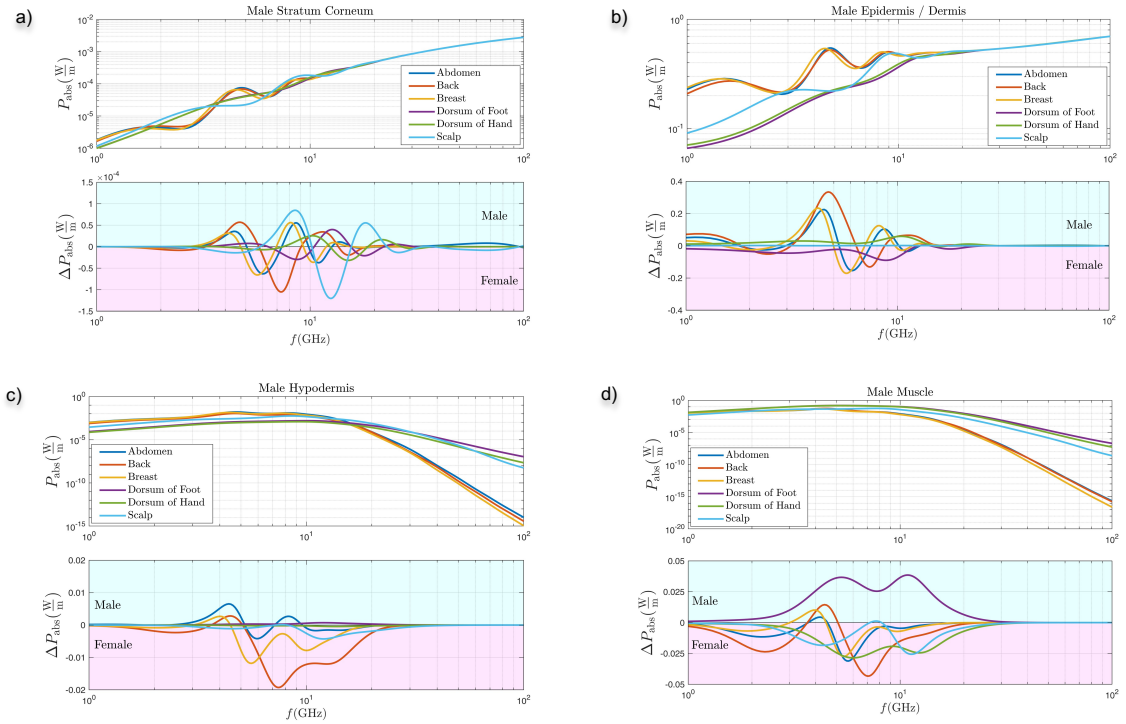

Fig.2: The integrated absorbed power in males' skin layers (top), and absorption difference between in genders' skin layers (bottom).

between 1-6 GHz, in which the penetration depths were larger than at higher frequencies. At 6 GHz, the electric field penetrated the hypodermis in the back, chest, and abdomen for both genders, with deeper penetration in males' body. Especially at 6 GHz, the highest penetration depth of the electric field was calculated as 9.9 mm in the males' breast, while it was as 8.5 mm in the females' breast. In the relatively thinner thicknesses of the foot (dorsum), hand (dorsum), and scalp, the electric field penetrated to the muscle in both genders. In all anatomical regions examined for both genders, the penetration depths at frequencies of 24 GHz and above were at maximum around 1.1 mm and thus confined to the epidermis/dermis layer. This highlights the need for thorough investigation into temperature increase in the epidermis/dermis, given the high-power absorption at these frequencies.

Acknowledgment: The research is funded by the German Federal Ministry of Education and Research (BMBF) in the course of the 6GEM research hub under grant number 16KISK038, and partially supported by the Swiss Research Foundation for Electricity and Mobile Communications (FSM) at ETH Zurich (Project No. A2019-01).

References

[1] M. H. Ross and W. Pawlina, *Histology : a text and atlas : with correlated cell and molecular biology*. Philadelphia: Wolters Kluwer/Lippincott Williams & Wilkins Health, 2011.

[2] P. Oltulu, B. Ince, N. Kokbudak, S. Findik, and F. Kilinc, "Measurement of epidermis, dermis, and total skin thicknesses from six different body regions with a new ethical histometric technique," *Turkish Journal of Plastic Surgery*, vol. 26, no. 2, p. 56-61, 2018, doi: https://doi.org/10.4103/tjps.tjps_2_17.

[3] M. C. Ziskin, S. I. Alekseev, K. R. Foster, and Q. Balzano, "Tissue models for RF exposure evaluation at frequencies above 6 GHz," *Bioelectromagnetics*, vol. 39, no. 3, pp. 173–189, Feb. 2018, doi: https://doi.org/10.1002/bem.22110.

[4] P. Störchle, W. Müller, M. Sengeis, S. Lackner, S. Holasek, and A. Fürhapter-Rieger, "Measurement of mean subcutaneous fat thickness: eight standardised ultrasound sites compared to 216 randomly selected sites," *Scientific Reports*, vol. 8, no. 1, Nov. 2018, doi: https://doi.org/10.1038/s41598-018-34213-0.

[5] T. Abe, R. W. Spitz, V. Wong, R. B. Viana, Y. Yamada, Z. W. Bell, R. N. Chatakondi, and J. P. Loenneke., "Assessments of facial muscle thickness by ultrasound in younger adults: absolute and relative reliability," *Cosmetics*, vol. 6, no. 4, p. 65, Nov. 2019, doi: 10.3390/cosmetics6040065.

[6] Sim4Life by ZMT. n.d. www.zurichmedtech.com.

Assessment of Temperature Changes caused by 7T MRI Scans using Proton Resonance Shift Thermometry

Maíra Martins Garcia[1,2], Daniel Erni[2], and Waldemar Zylka[1]

[1] Faculty of Electrical Engineering and Applied Natural Sciences, Westphalian University, D-45897Gelsenkirchen, Germany

[2] General and Theoretical Electrical Engineering (ATE), University of Duisburg-Essen, and CENIDE – Center of Nanointegration Duisburg-Essen, D-47048 Duisburg, Germany.

E-Mail: maira.b.garcia@studmail.w-hs.de

Abstract – Magnetic resonance (MR) thermometry is used to access the temperature of a subject during an MR imaging (MRI) procedure. Measuring temperature in MRI is notably important for analyzing the safety of the subject, for better control of an intentional or unintentional heating, for experimental validation of modelling results, among others, and it is especially relevant for MR applications in ultra-high fields (i.e. $B_0 \geq 7T$). There are different techniques used as MR thermometry, which are capable to acquire the subject's temperature locally and/or spatially. The proton resonance frequency (PRF) shift method presents high resolution, fast acquisition, non-invasiveness and relatively accurate results [1]. In this work, we used the PRF shift method to evaluate the temperature changes occurring in a muscle-mimicking phantom that was exposed to the radiofrequency (RF) heating applied by a birdcage head coil during a 7T MRI scanning. The temperature rise in the phantom's center was also measured using a digital thermometer. The results for both thermometer and PRF shift method (after the deduction of the B_0 drift effects) are comparable. They showed a temperature rise of the phantom by around 3°C after 112 minutes of applying a pulse sequence protocol, which was used to simultaneously heat the probe and acquire the phase information.

Methodology: The muscle-mimicking phantom is a water-gelatine-oil-salt mixture based in [2]. It was manufactured as described in [3], and the mixture was placed in a cylinder made of polymethyl methacrylate (PMMA, Plexiglas®, Germany) with 50 mm of radius and 200 mm of height (Fig. 1a). The phantom's dielectric properties were measured using a dielectric probe kit (DAK-12, SPEAG, Switzerland) equipment. Measurements for 300 MHz were repeated in 8 different regions of the phantom. The results for conductivity and permittivity ($\sigma_p = 0.742 \pm 0.006\ \mathrm{S/m}$; $\varepsilon_p = 57.65 \pm 0.45$) presented good agreement with literature values [4] and verified the phantom's homogeneity.
The MR measurements were done at a 7T MRI scanner (MAGNETOM 7T, Siemens Healthcare, Germany). A pulse-sequence protocol involving a combination of gradient-echo (GRE) and turbo spin-echo (TSE) sequences was implemented to acquire phase information for PRF shift and to heat the phantom, respectively. The GRE phase images were acquired before, after and between the TSE applications. A better description of this process and the sequences parameters are presented in [3]. To calculate the temperature increase of the phantom between time points t_f and t_0, for $t_f > t_0$, the

(a) (b) (c)

Fig.1: (a) Phantom and oil tubes inside the RF coil. (b) The measurement setup in the MR scanner. (c) Measuring the dielectric properties of the phantom mixture using the DAK equipment.

acquired GRE phases φ_0 and φ_f were used. The temperature difference ΔT_f was calculated using the PRF shift formula: $\Delta T_f = (\varphi_f - \varphi_0)/\alpha\gamma B_0 T_E$, for $\alpha = -0.01\ \mathrm{ppm/°C}$ (PRF coefficient), γ the gyromagnetic ratio of hydrogen and echo-time $T_E = 5.5\ \mathrm{ms}$. The phantom's phase variation comes mostly from the heating, but the fluctuations of the B_0 field during the measurement also counts for it. To dismiss the last one, four oil tubes ($h = 130\ \mathrm{mm}$; $r = 12\ \mathrm{mm}$) were measured along with the phantom, because the oil's phase vary predominately due to the B_0 drift. Finally, phase correction maps covering the region of the phantom were calculated interpolating the oil's phase changes, and the phantom's temperature variation was calculated as $\Delta T_f = ((\varphi_f - \varphi_0) - (\varphi_f^{oil} - \varphi_0^{oil}))/\alpha\gamma B_0 T_E$.

Results: The PRF shift temperature rise maps for the central axial slice were calculated for $t_f = 18, 31, 44, 56, 69, 82, 95, 108\ \mathrm{min}$. They are presented in Fig. 2 with and without B_0 drift corrections.

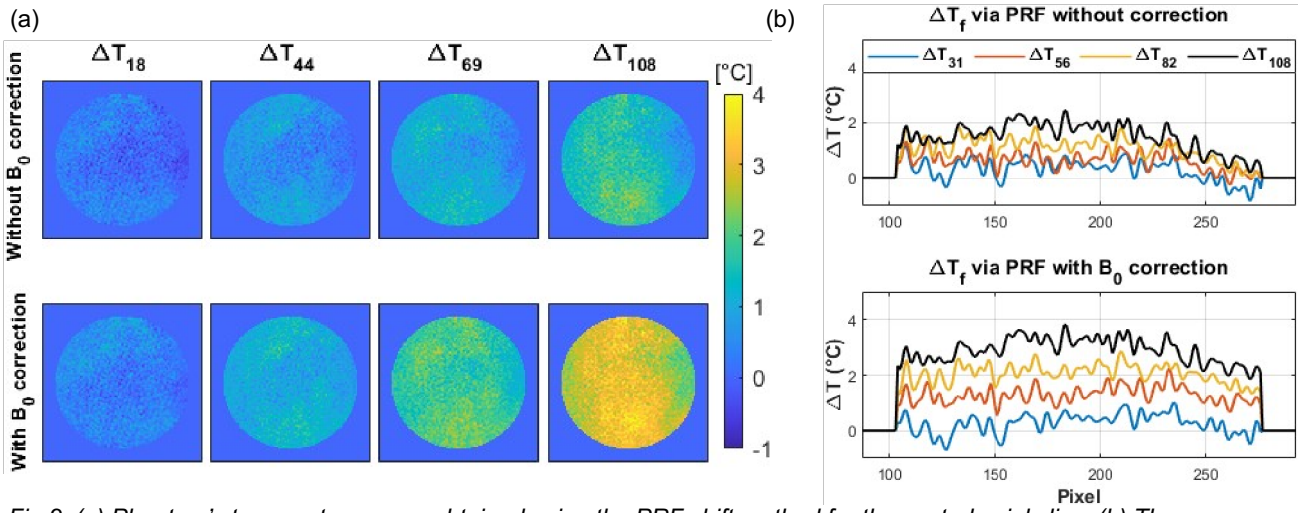

Fig.2: (a) Phantom's temperature maps obtained using the PRF shift method for the central axial slice. (b) The temperature variation along the horizontal line in the center of the phantom.

The central phantom's initial and final temperature was measured outside the MR room using the digital thermometer ($T_0 = 17.4 \pm 0.1\ °C$ and $T_{112} = 20.5 \pm 0.1\ °C$). Thermometer temperature values were linearly interpolated for the other t_f. Comparisons of thermometer and PRF shift method with B_0 drift corrections presented good accuracy, varying less than 0.5 °C.

Discussion and conclusion: This work used the PRF shift technique combined with thermometer measurements to asses the temperature rise of a muscle-mimicking phantom, which was exposed to RF heating applied by a birdcage head coil for 7T. This study presents limitations. Continuous temperature measurement, as well as a faster GRE acquisition could improve the accuracy of the technique. The PRF method used was successful to analyze the temperature rise spatiotemporally.

Acknowledgments: We thank the support from colleagues at the 7T MRI facilities at the University of São Paulo, São Paulo, Brazil, and the Otto von Guericke University, Magdeburg, Germany. MMG received funding from CAPES (process no. 88881.173609/2018-01) and the Westphalian University.

References

[1] N. De Zanche, C. Van den Berg, D. Brunner, et al., ISMRM best practices for safety testing of experimental rf hardware: http://www.ismrm.org/safety/RF_Hardware_Safety_Testing_2022-03.pdf (accessed Nov. 29, 2023).

[2] Y. Yuan, C. Wyatt, P. Maccarini, et al., "A heterogeneous human tissue mimicking phantom for RF heating and MRI thermal monitoring verification," *Physics in medicine and biology*, vol. 57, no. 7, pp. 2021–2037, 2012.

[3] M. M. Garcia, T. R. Oliveira, K. T. Chaim, et al., "Thermal measurements of a muscle-mimicking phantom during ultra-high field magnetic resonance imaging," *Current Directions in Biomedical Engineering*, vol. 9, no.1, pp.319-322, 2023.

[4] A. Hasgall, F Di Gennaro, C Baumgartner, et al., IT'IS database for thermal and electromagnetic parameters of biological tissues, version 4.1, Feb 22, 2022: http://itis.swiss/database (accessed Nov. 29, 2023).

Vat Photopolymerization 3D-Printing on Glass Substrates for the Fabrication of Microfluidic Systems

Frederik Morgenroth(1), Benedikt Emde(1), Lara Tickenbrock(1)

(1) Hamm-Lippstadt University of Applied Science
D-59065 Hamm, Germany

E-Mail: frederik.morgenroth@hshl.de
Web: www.hshl.de

Abstract – 3D printing offers compelling advantages in the field of microfluidics. Traditional methods of fabricating microfluidic systems are labor intensive, slow, and expensive, while being limited primarily to two-dimensional structures. 3D printing promises to reduce the lead time and cost of the manufacturing process, with the added benefit of producing three-dimensional structures. However, one major drawback of 3D printing systems is their lack of transparency. While vat photopolymerization resins can be translucent, their clarity is still too low for many analytical methods. A possible solution to this problem, a hybrid approach combining a glass substrate with a printed system, was investigated in this thesis. [1,2]

To test this approach, a Digital Light Processing printer was modified to accept glass substrates as part of the build plate. This allowed structures to be printed directly onto the substrate, with channel walls exposed to the glass, creating a transparent window into the system. Process parameters, including pre- and post-processing of the substrates and prints, were optimized to ensure adhesion to the substrate and high-quality print results. To this end, the substrates were silanized with Silane A 174 to increase the adhesion between the glass substrate and the 3D printed part. [3]

In this thesis it was demonstrated that the proposed hybrid approach is a viable method which can improve the optical access to 3D printed microchannels. Several test prints were designed and printed to generate a set of process parameters that can reliably print the desired structures.

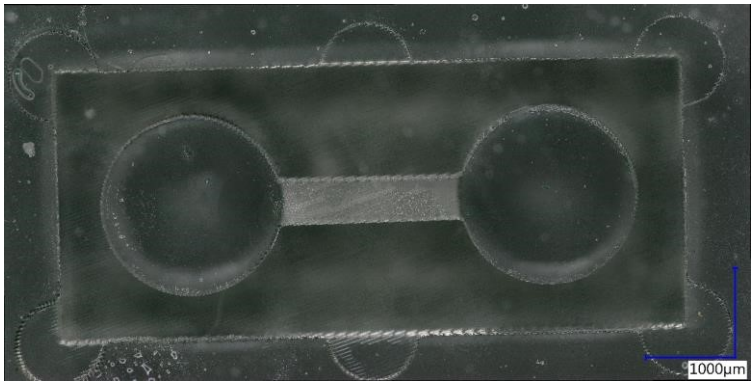

Fig. 1: Printed microchannel with a 0.5 mm x 0.5 mm cross section, as viewed from below, through the glass substrate.

Crucially, the post-processing of the prints required complete removal of uncured resin from the printed channel without releasing the print from the substrate. The most effective method for achieving this was to pull isopropyl alcohol through the channels using a vacuum, followed by a post-cure to solidify the remaining uncured resin.

To confirm the transparency and optical access to the channels, microscopy images of cells, as well as magnetic microbeads (3 µm), that were added to the channels, were taken. Both the beads and the cells could be observed through the substrate without issues.

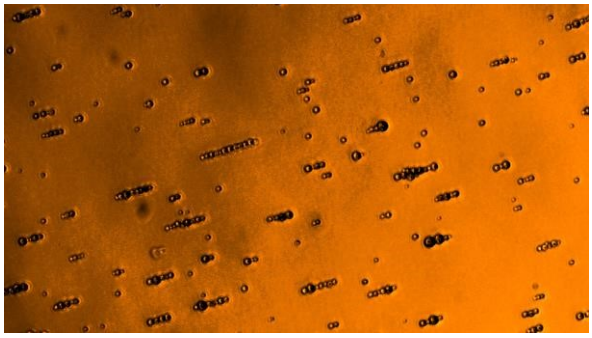

Fig. 2: Magnetic microbeads with a diameter of 3 µm inside the 3D printed microchannel. The image was taken from below the structure, through the glass substrate.

Furthermore, a passive microfluidic mixer was printed and evaluated, which allowed for observation of the interface between the two fluids. The inlet channels, as well as the mixing channel had a cross section of 0.5 mm x 0.5 mm. During operation the interface between the two fluids could be observed, while the diffusion of the fluids could be observed when the flow was reduced.

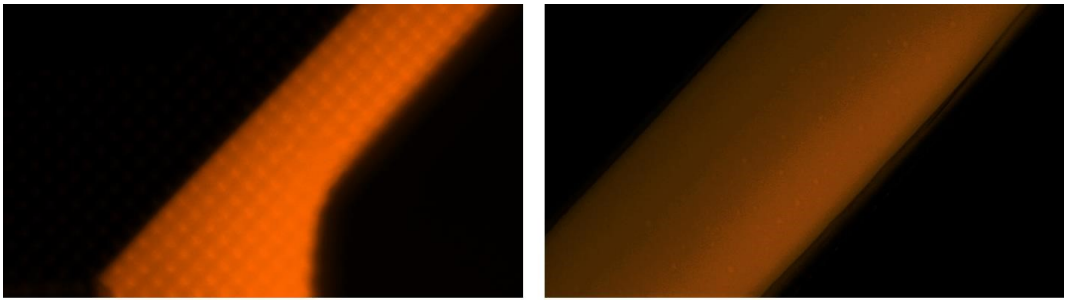

Fig. 3: Fluorescence imaging of the mixer during operation (left) and after turning off the pumps (right) and allowing to diffuse. The images were taken from below the structure, through the glass substrate.

References

[1] J. V. Crivello and E. Reichmanis, “Photopolymer materials and processes for Advanced Technologies,” *Chemistry of Materials*, vol. 26, no. 1, pp. 533–548, 2013. doi:10.1021/cm402262g

[2] M. Neubauer, M. McGlennen, S. Thomas, and S. Warnat, “3D printing on glass for direct sensor integration,” Engineering Research Express, vol. 1, no. 2, p. 025051, 2019. doi:10.1088/2631-8695/ab5e9f

[3] “3-(Trimethoxysilyl)propylmethacrylat ≥97%: Sigma-aldrich,” Sigma, https://www.sigmaaldrich.com/DE/de/product/sigma/m6514 (accessed Nov. 27, 2023).

Non-invasive analysis of hospital-acquired pneumonia by ion mobility & mass spectrometry in parallel

Hannah Schanzmann[1,2,3], Parviz Ahmad-Nejad[2], Veronika Ruzsanyi[4], Ursula Telgheder[3], and Stefanie Sielemann[1]

[1] Laboratory of Applied Instrumental Analytical Chemistry,
Hamm-Lippstadt University of Applied Sciences,
59063 Hamm, Germany

[2] Institute for Medical Laboratory Diagnostics,
Helios University Clinic Wuppertal with Witten/Herdecke University,
42283 Wuppertal/ 58455 Witten, Germany

[3] Department of Instrumental Analytical Chemistry,
University of Duisburg-Essen,
45141 Essen, Germany

[4] Institute for Breath Research,
University of Innsbruck,
6020 Innsbruck, Austria

E-Mail: hannah.schanzmann@hshl.de
Web: https://www.hshl.de/personen/hannah-schanzmann

Abstract
Hospital-acquired infections, like nosocomial pneumonia, are one of the greatest challenges in inpatient care. They lead to increased mortality, longer stays, higher treatment costs, and thus a socioeconomic burden [1]. Therefore, a rapid and reliable diagnostic is crucial for starting targeted antibiotic therapy. However, culture-based diagnostic procedures often take up to 48 hours to identify the causal pathogen [2].

Hence, a technology enabling faster detection of specific pathogenic agents needs to be developed. The project presented here aims to identify pathogens based on their specific microbiological volatile organic compound (mVOC) profiles in exhaled air. To measure these mVOCs from bacterial reference cultures and human breath, a benchtop system consisting of a thermal desorption (TD) gas chromatograph with a mass spectrometer (MS) is established. In addition, an ion mobility spectrometer (IMS) was coupled as a second detector in a way that the MS and the IMS shared the same flow line using a flow splitter. The coupling of TD-GC-MS-IMS has been built up for the first time. The workflow of the project aiming the non-invasive testing of nosocomial pneumonia based on breath analysis is illustrated in Fig. 1.

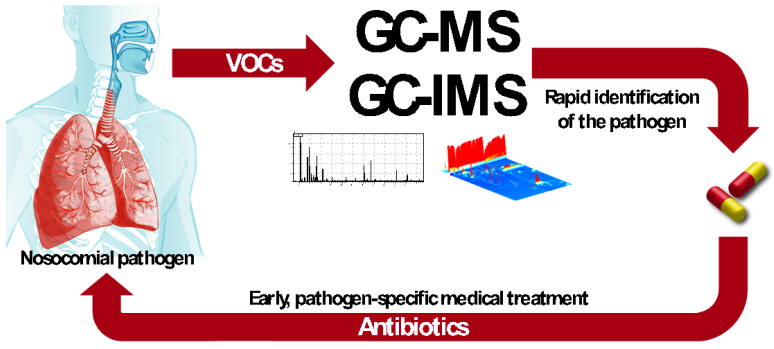

Fig.1: Overview of the planned workflow for establishing a non-invasive testing of the breath of patients with nosocomial pneumonia. With subsequent mass spectrometric and ion mobility spectrometric analysis, we aim to quickly identify the patient's lung pathogen to initiate antibiotic-specific therapy.

To find specific mVOCs as a benchmark of selected known pathogens such as *Pseudomonas aeruginosa*, *Staphylococcus aureus*, *Streptococcus pneumonia*, *Legionella pneumophilia*, *Acinetobacter baumannii complex*, and *Escherichia coli* grown in vitro the volatiles in the culture's headspace were extracted onto TD tubes using a self-made sampling chamber. Then, the TD tubes were subsequently measured with the TD-GC-MS-IMS. Furthermore, as the sampling chamber contains an incubator, freshly inoculated agar plates can be measured continuously during their growth phase.

Initial measurements of selected pathogens demonstrate the great advantage of the new coupling: identifying unknowns in the IMS measurements using the mass spectrometric database, as there are still no databases for IMS available. For example, Indole can be found in the headspace of *Escherichia coli* culture, which has been shown to be a product of its tryptophan metabolism. We could show that specific peaks can be detected already after six hours of incubation.
The next step will be performing a proof of principle trial in the clinical setting, examining a patient's breath profile with nosocomial infections, and comparing the volatile fingerprints obtained in the in vitro studies.

References

[1] E. H. Ibrahim, S. Ward, G. Sherman, and M. H. Kollef, "A comparative analysis of patients with early-onset vs late-onset nosocomial pneumonia in the ICU setting," *Chest*, vol. 117, no. 5, pp. 1434–1442, May 2000.

[2] K. Dalhoff et al., "Epidemiology, diagnosis and treatment of adult patients with nosocomial pneumonia – update 2017," *Pneumologie*, vol. 72, no. 01, pp. 15–63, Jan. 2018.

Magnetic biosensing with magnetic nanoparticles: Simulative approach to predict signal intensity in frequency mixing magnetic detection

Beril Simsek[(1)], Hans-Joachim Krause[(1),(2)] and Ulrich M. Engelmann[(1)]

[(1)] Medical Engineering and Applied Mathematics,
FH Aachen University of Applied Sciences,
D-52428 Jülich, Germany
[(2)] Institute of Biological Information Processing,
Bioelectronics (IBI-3), Forschungszentrum Jülich,
D-52428 Jülich, Germany
E-Mail: beril.simsek@alumni.fh-aachen.de | engelmann@fh-aachen.de

Magnetic nanoparticles (MNP) are investigated with great interest for biomedical applications in diagnostics (e.g. imaging: magnetic particle imaging (MPI)), therapeutics (e.g. hyperthermia: magnetic fluid hyperthermia (MFH)) and multi-purpose biosensing (e.g. magnetic immunoassays (MIA)). What all of these applications have in common is that they are based on the unique magnetic relaxation mechanisms of MNP in an alternating magnetic field (AMF). While MFH and MPI are currently the most prominent examples of biomedical applications, here we present results on the relatively new biosensing application of frequency mixing magnetic detection (FMMD) from a simulation perspective. In general, we ask how the key parameters of MNP (core size and magnetic anisotropy) affect the FMMD signal: by varying the core size, we investigate the effect of the magnetic volume per MNP; and by changing the effective magnetic anisotropy, we study the MNPs' flexibility to leave its preferred magnetization direction. From this, we predict the most effective combination of MNP core size and magnetic anisotropy for maximum signal generation.

In the specific technique of FMMD, two AMF are applied in superposition [1]: the low-frequency (f_1) magnetic driving field with high field amplitude (H_1), which drives MNP close to saturation, and the high-frequency (f_2) excitation field with low field amplitude (H_2), which probes MNP susceptibility:

$$H(t) = H_0 + H_1 \sin(2\pi f_1 \cdot t) + H_2 \sin(2\pi f_2 \cdot t) \qquad (1)$$

As can be seen in equation (1), a static offset field, H_0, is applied, which is the parameter being varied in FMMD measurements.

Resulting from the nonlinear magnetization of the MNP, harmonics of both individual incident frequencies as well as intermodulation products of these frequencies are generated. In this work, we use dynamic magnetization simulations including stochastic temperature fluctuations in the MNP relaxation process by solving the Landau-Lifshitz-Gilbert (LLG) equation to predict FMMD signals:

$$\frac{dm_p}{dt} = \frac{\mu_0 \gamma}{1+\alpha^2} \cdot \left(H_{eff} \times m_p + \alpha m_p \times \left(H_{eff} \times m_p \right) \right) \qquad (2)$$

Details on the method are found in [2, 3].

Below we show simulation results for the FMMD signal of the first intermodulation signal $f_1 + f_2$: LEFT for varying core sizes ($d_C = 12, 16, 20, 24, 28$ nm) at fixed (bulk) magnetic anisotropy ($K = -11$ kJ/m³) and RIGHT for varying magnetic anisotropy ($K = -5, -9, -11, -13, -17$ kJ/m³) at fixed core sizes ($d_C = 20$ nm and $d_C = 28$ nm).

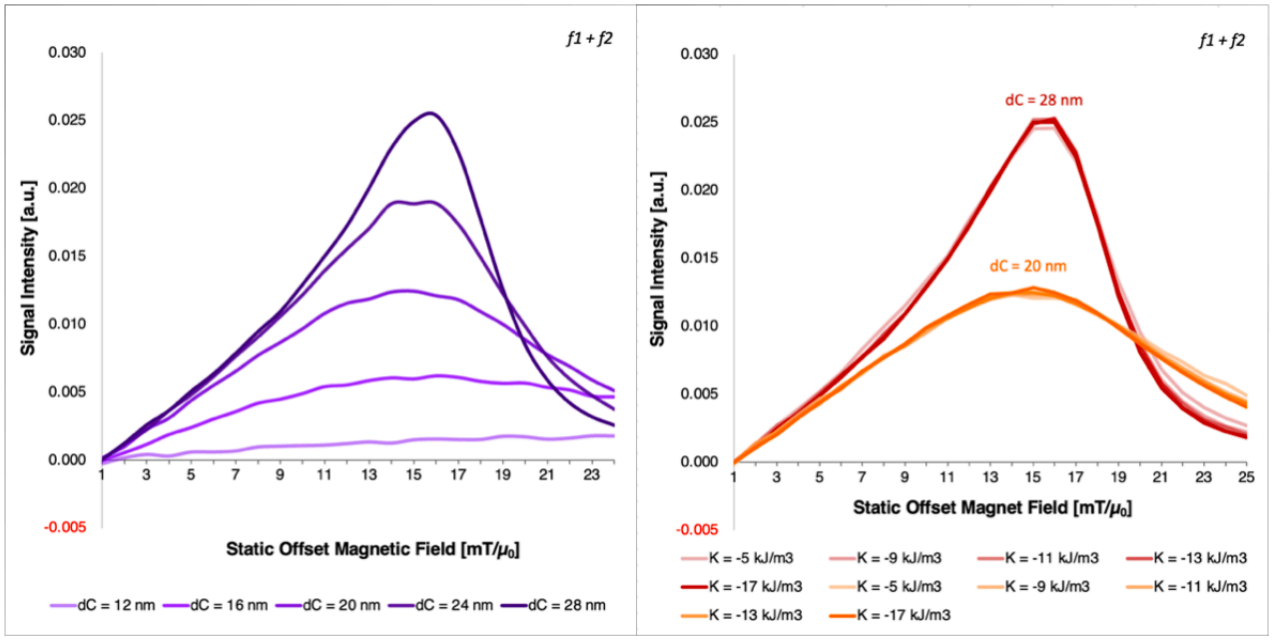

In the left figure, one can see that larger core sizes generally increase signal intensity, which is consistent with predictions for MPI and MFH [4, 5] and has recently been confirmed experimentally and predictively for FMMD [6]. On the contrary, preliminary magnetic anisotropy results shown in the right figure suggest that the FMMD signal intensity is independent of magnetic anisotropy. Both predictions involve a lognormal size distribution of MNP. The effect of core size presumably dominates the effect of magnetic anisotropy. These preliminary findings need to be further investigated with wider parameter variation, as magnetic particle core size and magnetic anisotropy are expected to be interdependent, to finally identify the MNP that are best suited for magnetic biosensing applications using FMMD.

References

[1] U. M. Engelmann, A. Shalaby, C. Shasha, K. M. Krishnan, and H.-J. Krause, “Comparative Modeling of Frequency Mixing Measurements of Magnetic Nanoparticles Using Micromagnetic Simulations and Langevin Theory,” *Nanomaterials (Basel, Switzerland)*, vol. 11, no. 5, 2021, doi: 10.3390/nano11051257.

[2] C. Shasha and K. M. Krishnan, “Nonequilibrium Dynamics of Magnetic Nanoparticles with Applications in Biomedicine,” *Advanced materials*, e1904131, 2020, doi: 10.1002/adma.201904131.

[3] U. M. Engelmann, C. Shasha, and I. Slabu, “Magnetic nanoparticle relaxation in biomedical application: focus on simulating nanoparticle heating,” *Magnetic Nanoparticles in Human Health and Medicine: Current Medical Applications and Alternative Therapy of Cancer*, pp. 327–354, 2021.

[4] U. M. Engelmann *et al.,* “Magnetic relaxation of agglomerated and immobilized iron oxide nanoparticles for hyperthermia and imaging applications,” *IEEE Magnetics Letters*, vol. 9, pp. 1–5, 2018.

[5] U. M. Engelmann, C. Shasha, E. Teeman, I. Slabu, and K. M. Krishnan, “Predicting size-dependent heating efficiency of magnetic nanoparticles from experiment and stochastic Néel-Brown Langevin simulation,” *Journal of Magnetism and Magnetic Materials*, vol. 471, pp. 450–456, 2019, doi: 10.1016/j.jmmm.2018.09.041.

[6] U. M. Engelmann, A. M. Pourshahidi, A. Shalaby, and H.-J. Krause, “Probing particle size dependency of frequency mixing magnetic detection with dynamic relaxation simulation,” *Journal of Magnetism and Magnetic Materials*, vol. 563, p. 169965, 2022, doi: 10.1016/j.jmmm.2022.169965.

Effect of different cannula positions in the pulmonary artery on blood flow and gas exchange using computational fluid dynamics analysis

Annika Schmitz[(1)], Shah Eiman Amzar Shah Apandi[(1)], Jan Spillner[(2)], Flutura Hima[(2)], Mehdi Behbahani[(1)]

[(1)] Institute for Bioengineering (IfB),
Faculty for Medical Engineering and Techno-Mathematics, University of Applied Sciences Aachen,
52428 Jülich, Germany

[(2)] Department of Thoracic and Cardiovascular Surgery
Medical Faculty, University Hospital RWTH Aachen,
52074 Aachen, Germany

E-Mail: annika.schmitz@alumni.fh-aachen.de

Abstract – Pulmonary arterial cannulation is a common and effective method for percutaneous mechanical circulatory support for concurrent right heart and respiratory failure [1]. However, limited data exists to what effect the positioning of the cannula has on the oxygen perfusion throughout the pulmonary artery (PA). This study aims to evaluate, using computational fluid dynamics (CFD), the effect of different cannula positions in the PA with respect to the oxygenation of the different branching vessels in order for an optimal cannula position to be determined. The four chosen different positions (see Fig. 1) of the cannulas are, in the lower part of the main pulmonary artery (MPA), in the MPA at the junction between the right pulmonary artery (RPA) and the left pulmonary artery (LPA), in the RPA at the first branch of the RPA and in the LPA at the first branch of the LPA.

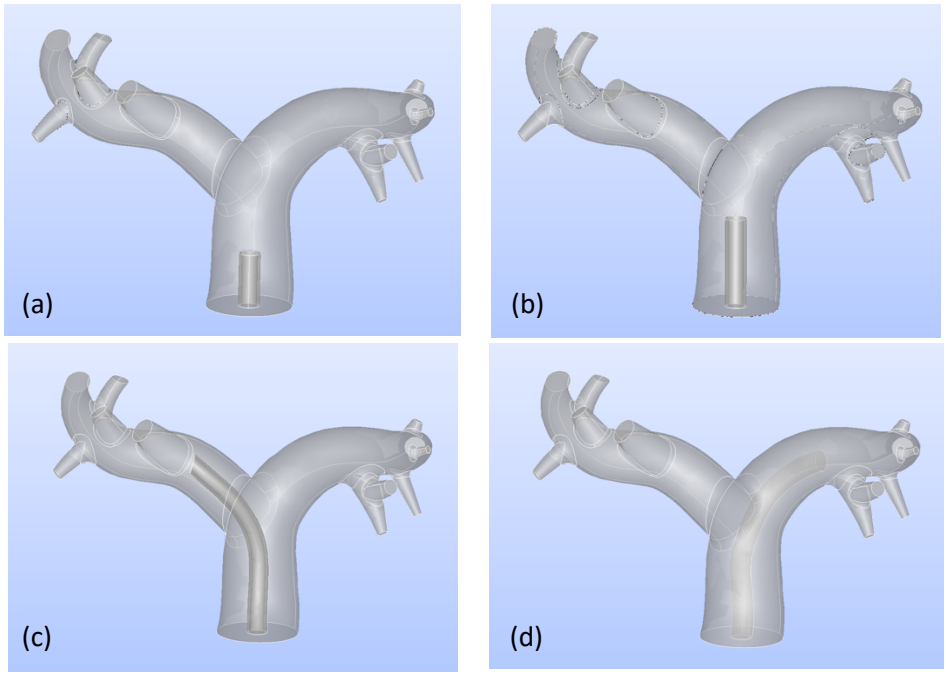

Fig.1: 3D model of the pulmonary artery with the 11 outflowing branching blood vessels, with position of (a) cannula in the main pulmonary artery, (b) in the main pulmonary artery at the junction between the right and left pulmonary, (c) artery cannula in right pulmonary artery and (d) cannula in the left pulmonary artery

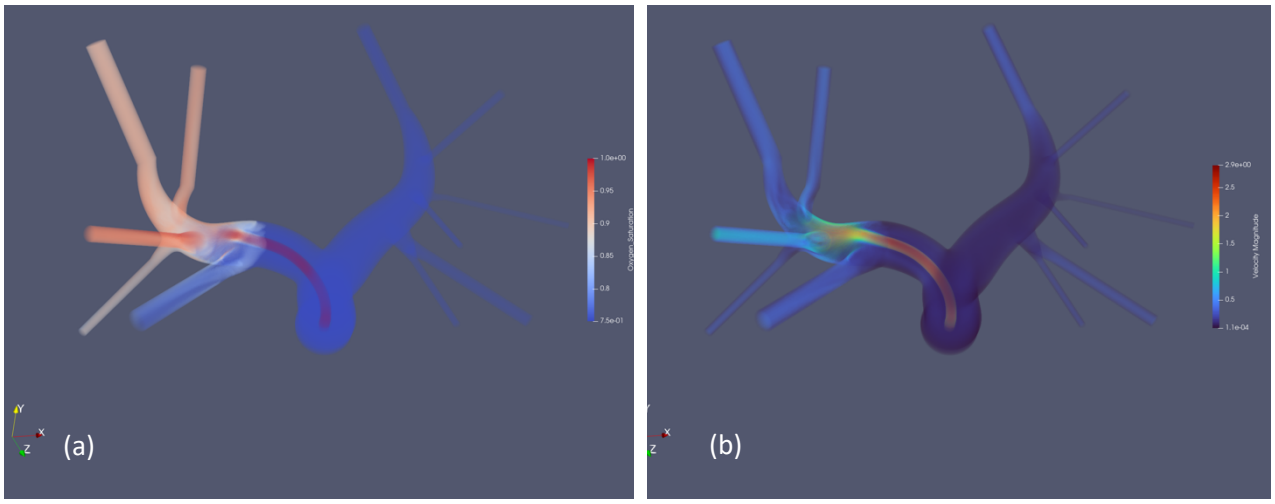

Fig.2: Preliminary computational results showing (a) the oxygen saturation distribution and (b) the velocity profile of the blood flow for a right pulmonary artery cannulation with 50% veno-arterial support level

Pulmonary artery geometries are created from individual patient CT-data and processed further using different non-commercial and commercial STL and STEP specific processing and editing software for 3D triangular meshes. Extraction of the geometry from CT-data is particularly challenging as arterial and venous blood vessels intertwine, hence the PA was reconstructed using a 3D geometry with 11 outflowing vessels of the PA. Code_Saturne, an open-source software, was used for the CFD analysis and based on the results of the flow field, the equations for oxygen concentration distribution are also solved. The post-processing of the simulation is also performed using an open-source platform, ParaView.

Preliminary computational results reveal how different cannula positions have a strong influence on the blood flow patterns and which positions are more favorable than others based on the oxygen saturation distribution. Veno-arterial support levels of 50% and 90% from the total blood flow rate are also set as parameters for this study, which influences the results [2]. The individual geometry of the patient is also assumed to not only have a major impact on the computational results but also in the modelling accuracy which became evident in the geometry building process from CT data, due to the complex geometry and difficulty in separating closely positioned small arteries, calling for the use of specific tools. Hence, the remodeling of extracted and edited patient data geometry may also be necessary in future studies in order to provide better understanding and further advantages.

References

[1] C. Huang, C. Wang, H. Chou, N. Chi, H. Yu, and Y. Chen, "Role of percutaneous pulmonary cannulation in extracorporeal life support for acute cardiac failure: A single-center case series," *Artificial Organs.*, vol. 47, no. 1, pp. 205-213, 2023.

[2] D. Malinowski, Y. Fournier, A. Horbach, M. Frick, M. Magliani, S. Kalverkamp, M. Hildinger, J. Spillner, M. Behbahani and F. Hima, "Computational fluid dynamics analysis of endoluminal aortic perfusion," *Perfusion*, vol. 38, no. 6,, pp. 1-8, 2022

[3] F. Capuano, Y.-H. Loke, and E. Balaras, “Blood Flow Dynamics at the Pulmonary Artery Bifurcation,” *Fluids*, vol. 4, no. 4, p. 190, Nov. 2019, doi: 10.3390/fluids4040190

[4] A. D. Bordones et al., “Computational fluid dynamics modeling of the human pulmonary arteries with experimental validation,” *Annals of Biomedical Engineering*, vol. 46, no. 9, pp. 1309–1324, 2018. doi:10.1007/s10439-018-2047-1

[5] B. T. Tang et al., “Wall shear stress is decreased in the pulmonary arteries of patients with pulmonary arterial hypertension: An image-based, Computational Fluid Dynamics Study,” *Pulmonary Circulation*, vol. 2, no. 4, pp. 470–476, 2012. doi:10.4103/2045-8932.105035

EEM spectroscopy characterization of humic substances of biomedical importance

Dinara Sherelkhan [1,2] and Alina Alibekova [1]

[1] Institute of Ecological Problems, Al-Farabi Kazakh National University, Almaty 050040, Kazakhstan

[2] Institute for Bioengineering, FH Aachen University of Applied Sciences, 52428 Jülich, Germany,

E-Mail: sherelkhandinara@gmail.com

Humic substances possess distinctive chemical features enabling their use in many advanced applications, including biomedical fields. No chemicals in nature have the same combination of specific chemical and biological properties as humic substances. Traditional medicine and modern research have demonstrated that humic substances from different sources possess immunomodulatory and anti-inflammatory properties, which makes them suitable for the prevention and treatment of chronic dermatoses, allergic rhinitis, atopic dermatitis, and other conditions characterized by inflammatory and allergic responses [1-4]. The use of humic compounds as agents with antifungal and antiviral properties shows great potential [5-7].

However, the biological activity of humic substances demonstrated in laboratory investigations precludes their broad application in biomedicine. Manufacturers of humic-based drugs/medicines claim various therapeutic characteristics not supported by preclinical and clinical trial outcomes. Humic compound-based drugs lack widespread recognition owing to the challenges associated with their standardization. Preclinical drug development includes defining the active component's nature/structure and the best methodologies/strategies for quality control standardization. Understanding the composition and structure of humic compounds is insufficient to apply them in pharmacology [8]. Humic substance's solubility, reactivity, and biological activity are affected by the circumstances under which they are formed, the procedures used to isolate them from natural sources, and the structure/weight of macromolecules.

Difficulties in determining the heterogeneous nature and multifunctional properties of humic substances have led to the need for employing advanced techniques. Fluorescence techniques are often regarded as very precise and sensitive. Excitation and emission spectra are combined to give better depth to research data and may provide crucial new insight [9]. Our goal was to investigate the excitation-emission matrix (EEM) characteristics of humic substances extracted from lignite (LHS) and soil (SHS) samples.

An ordinary EEM contour map of LHS is depicted using fluorescence peaks of maximum intensity, which are indicative of the specific fluorophores or functional groups involved (Figure 1).

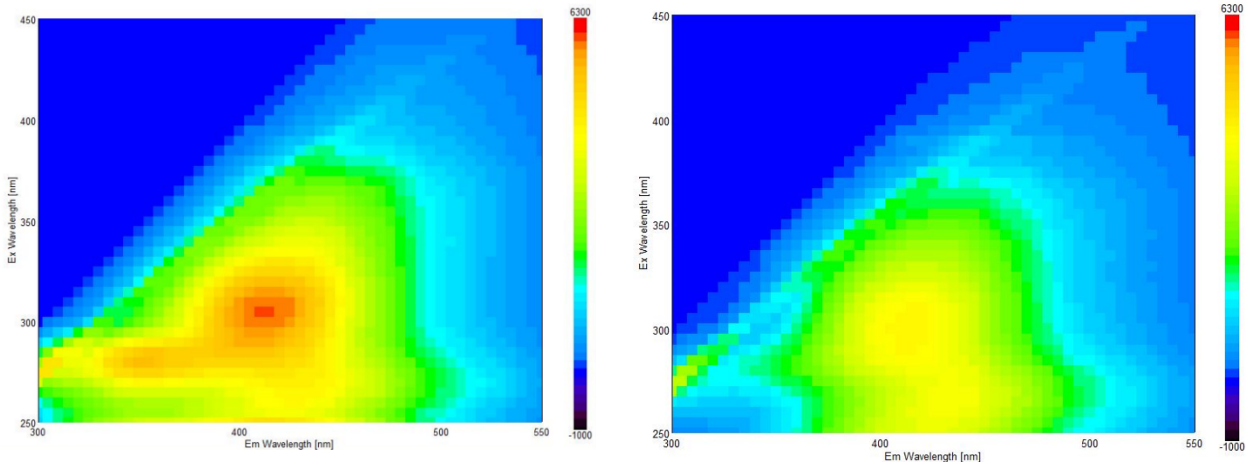

Fig.1: Fluorescence excitation/emission matrix of lignite-derived LHS (a) and soil-derived SHS (b) humic substances.

Strong fluorophores (excitation/emission) are detected at 270/445nm. Eight general categories of fluorescence peaks were postulated by P.G. Coble [10], including pigment-like, protein-like, and humic-like fluorescence signatures. The maximal peaks observed in the current investigation are located in the area designated as "A peak," which corresponds to the humic-like substances. The dispersion of the LHS peak within the wavelength range of 275/440–450 nm was likely attributable to their heterogeneous composition. Due to the evident similarity between the EEMs of LHS and SHS, all peaks are classified as humic-like. Nevertheless, the marginal fluctuations in peak positions that were noted suggest subtle variations in the composition of humic substances among the samples. This shows that LHS possesses aromatic structures consisting of three to four rings. The findings indicate that humic substances derived from different sources can be properly characterized using EEM spectroscopy, which is important as the process of drug development utilizing humic substances entails the examination of their various chemical and pharmacological characteristics and establishing standards.

References

1. S.L. Khil'ko, I.V. Efimova, and O.V. Smirnova, "Antioxidant properties of humic acids from brown coal." *Solid Fuel Chemistry*, vol. 45**, no.** 6, pp. 367-371, 2011.
2. V. Vetvicka, et al., "Glucan and humic acid: synergistic effects on the immune system." *J Med Food*, vol. 13, no. 4, pp. 863-869, 2010.
3. E.S. Trofimova, et al., "Anti-allergic properties of humic acids isolated from pine-sphagnum-cotton sedge peat." *Bull Exp Biol Med,* vol. 172, no. 3, pp. 324-327, 2022.
4. T.S. Murbach, et al., "A toxicological evaluation of a fulvic and humic acids preparation." *Toxicol Rep*, vol. 7**,** pp. 1242-1254. 2022.
5. B. Allard, H. Borén, and A. Grimvall (Eds.). *Humic substances in the aquatic and terrestrial environment: proceedings of an international symposium, Linköping, Sweden, August 21-23, 1989*. Berlin, Heidelberg: Springer 1991.
6. G. Kornilaeva, I. Perminova, and E. Karamov. "Humic substances as active anti HIV components for microbicides." in *Abstract Book of the First International Conference on Humics based Innovative Technologies «Natural and Synthetic Polyfunctional Compounds and Nanomaterials in Medicine and Biomedical Technologies*. 2010.
7. M. Hafez, et al., "Humic substances as an environmental-friendly organic wastes potentially help as natural anti-virus to inhibit COVID-19." *Sci. Arch*, vol. 1, pp. 53-60, 2020.
8. S. Hriciková, et al., "Humic substances as a versatile intermediary. *Life (Basel)*, vol. 13, no. 4, p. 858, 2023.
9. L. Doskočil, et al., "Spectral characterization and comparison of humic acids isolated from some European lignites." *Fuel*, vol. 213, pp. 123-132, 2018.
10. P.G. Coble, "Characterization of marine and terrestrial DOM in seawater using excitation-emission matrix spectroscopy." *Marine Chemistry*, vol. 51, np. 4,: pp. 325-346, 1996.

AstroBioLab: Review of Technical and Bioanalytical Approaches

Atakan Tepecik(1)

(1) Institute for Bioengineering
FH Aachen
Heinrich Mußmann Str.1
Jülich 52428 Germany
E-Mail: tepecik@fh-aachen.de
Web: https://www.fh-aachen.de/forschung/institute/ifb/

Abstract –This study presents the concept of AstroBioLab, an autonomous astrobiological field laboratory tailored for the exploration of (sub)glacial habitats. AstroBioLab is an integral component of the TRIPLE (Technologies for Rapid Ice Penetration and subglacial Lake Exploration) DLR-funded project, aimed at advancing astrobiology research through the development and deployment of innovative technologies. AstroBioLab integrates diverse measurement techniques such as fluorescence microscopy, DNA sequencing and fluorescence spectrometry, while leveraging microfluidics for efficient sample delivery and preparation.

AstroBioLab is designed as an instrument for approaching fundamental questions regarding the existence and adaptability of life in extreme environments, with Antarctica serving as a terrestrial analogue to extraterrestrial habitats. Its integration into the TRIPLE project should facilitate the investigation of Antarctic ecosystems, shedding light on the limits and adaptations of life under extreme conditions.

Through its autonomous operation, AstroBioLab should minimize human intervention, optimize efficiency and reduce contamination risks. State-of-the-art automation systems and advanced artificial intelligence algorithms should enable automated sample handling and analysis. This approach ensures the integrity of pristine environments and streamlines data acquisition.

To comprehensively assess the collected environmental samples, AstroBioLab will employ a suite of measurement techniques. Fluorescence microscopy enables the visualization and identification of microbial life, providing valuable morphological insights. DNA sequencing elucidates the genetic diversity and phylogenetic relationships of the detected microorganisms, enhancing our understanding of their evolutionary origins and adaptation strategies. Furthermore, fluorescence spectrometry assists in identification and quantification of specific biomarkers, thus offering valuable information about the biochemical processes within the samples.

Sample delivery and preparation will be performed using microfluidics-based systems. Due to precise fluid control and manipulation, microfluidics technology enables efficient handling of small sample volumes and reagents. This allows rapid and accurate sample processing, minimizes contamination and facilitates high-throughput functioning.

The integration of AstroBioLab into the TRIPLE project represents a significant advancement in the exploration of extreme environments and in the search for extraterrestrial life. By combining autonomous operation, synergy in measurement techniques and microfluidic-based sample handling, AstroBioLab provides a powerful platform for studying and characterizing microbial life in Antarctica. The findings from this project should contribute to our understanding of the potential habitability of other celestial bodies and promote future astrobiological explorations.

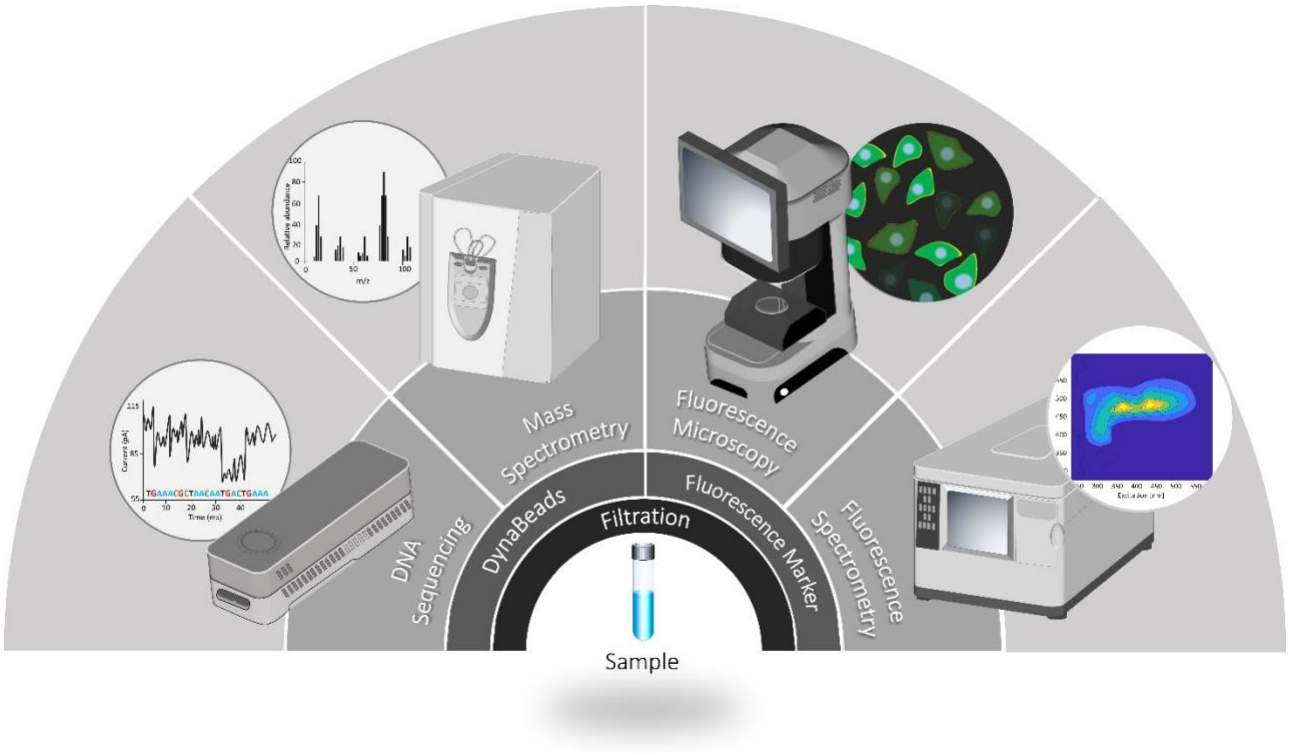

Fig.1: Schematic visualization of the proposed AstroBioLab systems. Graphic Credit: Dr. Nuraly S. Akimbekov.

Poster Sessions

On-site treatment of hospital wastewater in a full-scale treatment plant in Germany: Evaluation of treatment performance

Sarah Häußer [1,2], Martin Weber [4], Christian Mauer [5], Volker Linnemann [3], Anna Pfannstiel [2], Johannes Pinnekamp [3], Thomas Wintgens [3], Claudia Klümper [1], and Silvio Beier [2]

[1] Department Hamm 2, Hamm-Lippstadt University of Applied Sciences,
D-59063 Hamm, Germany
[2] Bauhaus-Institute for infrastructure solutions (b.is), Bauhaus-Universität Weimar,
D-99423 Weimar, Germany
[3] Institute of Environmental Engineering, RWTH Aachen University,
D-52074 Aachen, Germany
[4] Aggerverband,
D-51645 Gummersbach, Germany
[5] Weber-Ingenieure GmbH,
D-75177 Pforzheim, Germany
E-Mail: sarah.haeusser@hshl.de, silvio.beier@uni-weimar.de

Abstract
Hospital wastewater containing harmful compounds such as pharmaceuticals, disinfectants, viruses and antibiotic resistance genes is a major environmental and health concern [1]. Despite several laboratory-scale studies, few pilot or industrial-scale studies have been published [1–4]. In Haeusser et al. [3], we investigated the elimination performance of a large-scale hospital wastewater treatment plant (HWTP). For the first time a full-scale, on-site treatment plant at a hospital in Germany, consisting of a membrane bioreactor and a subsequent ozonation was evaluated with regard to the elimination of pharmaceutical residues, standard chemical-physical parameters, microbiological parameters, and SARS-CoV-2 RNA fragments. For this purpose, 24 h composite samples were taken up to twice a week over a period of six weeks between April 2021 and June 2021 from the influent and effluent of the (HWTP). In addition to the standard physicochemical parameters, SARS-CoV-2 RNA fragments, and the microbiological parameters *Escherichia coli* and Enterococci were analyzed. Furthermore, the following drug residues and trace substances were analyzed: bisoprolol, telmisartan, metoprolol, metoprolol acid, diclofenac, ibuprofen, tramadol, carbamazepine, ciprofloxacin, clarithromycin and sulfamethoxazole.

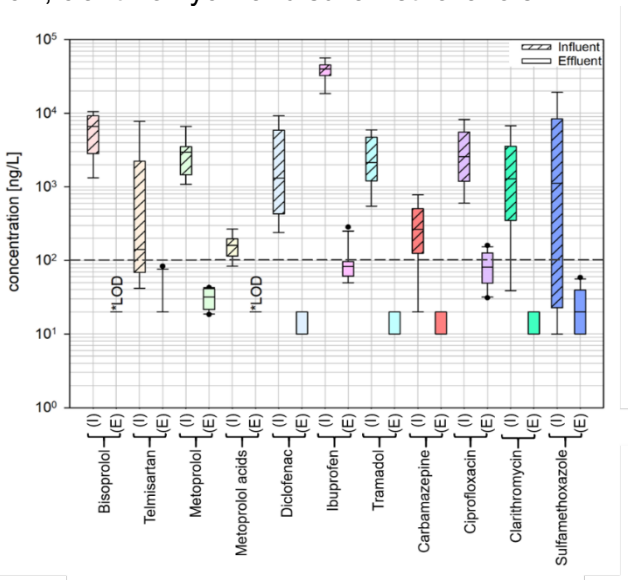

*Figure 1: Boxplots with median of the concentration of pharmaceutical residues in the (I) influent (n=9) and (E) effluent (n=11) of the hospital WWTP. The dashed line shows the General Precautionary Value of 100 ng/L for drinking water quality of the Federal Environment Agency. *LOD= Limit of quantification.*

Our results demonstrate that after ten years of stable operation, the treatment plant works highly efficiently regarding the elimination of pharmaceuticals and bacterial indicators. Hence, elimination in pilot-scale could be confirmed in full-scale and after ten years of operation [5, 6]. For microbiological parameters log reductions of up to 6 log_{10} were achieved. SARS-CoV-2 RNA fragments could be detected and quantified in the influent but not in the effluent of HWTP. In Figure 1, most concentrations of pharmaceutical residues in the HWTP effluent were well below 100 ng/L after treatment. Only the maximum effluent concentrations of ibuprofen and ciprofloxacin had higher values in the effluent. Elimination rates were above 90 % for all pharmaceutical residues and ranged from 91.5 % (Telmisartan) to 99.7 % (Bisoprolol). These data are comparable to results from other studies investigating separate hospital wastewater treatment in full- or pilot-scale [4, 7].

Currently, micropollutants and emerging contaminants, including pharmaceutical residues, are not regulated in the European Water Frame Work Directive or Urban Wastewater Treatment Directive. For this reason, the Swiss Water Protection Ordinance (GSchV 2016) was used to assess the elimination performance of sulfamethoxazole, clarithromycin, ciprofloxacin, diclofenac, carbamazepine and metoprolol. Municipal wastewater treatment plants in Switzerland must eliminate 80% of Contaminants of Emerging Concern. Elimination rates in our study would fulfill this requirement. Regarding drinking water quality, the German Environmental Agency recommends a general precautionary value of 100 ng/L, and for some pharmaceutical residues, there are also health-related guidance values for drinking water. These values are derived for drinking water and not treated wastewater, but are considered reasonable for evaluating the elimination performance of HWTP. Only the maximum effluent concentrations of ibuprofen and ciprofloxacin sometimes exceed the general precautionary value of 100 ng/L. However, in Germany, the health-related guidance value for drinking water is 1 µg/L. Thus, from a human health perspective, concentrations in treated hospital wastewater are acceptable.

In conclusion this study demonstrates that separate and advanced treatment of hospital wastewater has the potential to efficiently reduce pharmaceuticals, microorganisms, and specific gene fragments into the municipal sewer system. As containment of antimicrobial resistance and its spread in the environment is an urgent challenge in public health we will address this issue in our future study in which we plan to investigate the performance of the hospital wastewater treatment plant with regard to antimicrobial resistance.

References

[1] A. Majumder, A. K. Gupta, P. S. Ghosal, and M. Varma, "A review on hospital wastewater treatment: A special emphasis on occurrence and removal of pharmaceutically active compounds, resistant microorganisms, and SARS-CoV-2," *Journal of environmental chemical engineering*, vol. 9, no. 2, p. 104812, 2021, doi: 10.1016/j.jece.2020.104812.

[2] M. I. Pariente *et al.,* "Critical review of technologies for the on-site treatment of hospital wastewater: From conventional to combined advanced processes," *Journal of environmental management*, vol. 320, p. 115769, 2022, doi: 10.1016/j.jenvman.2022.115769.

[3] S. Haeusser *et al.,* "On-site treatment of hospital wastewater in a full-scale treatment plant in Germany: SARS-CoV-2 and treatment performance," *Water science and technology : a journal of the International Association on Water Pollution Research*, vol. 87, no. 7, pp. 1747–1763, 2023, doi: 10.2166/wst.2023.088.

[4] P. Ajo, S. Preis, T. Vornamo, M. Mänttäri, M. Kallioinen, and M. Louhi-Kultanen, "Hospital wastewater treatment with pilot-scale pulsed corona discharge for removal of pharmaceutical residues," *Journal of environmental chemical engineering*, vol. 6, no. 2, pp. 1569–1577, 2018, doi: 10.1016/j.jece.2018.02.007.

[5] S. Beier, C. Cramer, C. Mauer, S. Köster, H. F. Schröder, and J. Pinnekamp, "MBR technology: a promising approach for the (pre-)treatment of hospital wastewater," *Water science and technology : a journal of the International Association on Water Pollution Research*, vol. 65, no. 9, pp. 1648–1653, 2012, doi: 10.2166/wst.2012.880.

[6] S. Beier *et al.,* "Full scale membrane bioreactor treatment of hospital wastewater as forerunner for hot-spot wastewater treatment solutions in high density urban areas," *Water science and technology : a journal of the International Association on Water Pollution Research*, vol. 63, no. 1, pp. 66–71, 2011, doi: 10.2166/wst.2011.010.

[7] U. Nielsen, *Full scale advanced wastewater treatment at Herlev hospital treatment performance and evaluation: hospital treatment performance and evaluation.* [Online]. Available: https://www.dhigroup.com/global/news/2016/08/hospital-wastewater-from-a-pollution-problem-to-new-water-resources (accessed: Mar. 3 2022).

Acknowledgements: The authors would like to thank the Waldbröl District Hospital and the laboratory teams at the ISA of RWTH Aachen University and Hamm-Lippstadt University of Applied Sciences for their excellent collaboration.

Development of a breast phantom to validate a novel patient positioning system for breast cancer radiotherapy

Ganna Papakina [(1)], Frederik Morgenroth [(1)], Jürgen Trzewik [(1)] and Marvin Christopher Stegmann [(1,2)]

[(1)] Hamm-Lippstadt University of Applied Sciences,
D- 59063 Hamm, Germany

[(2)] GermanPhysics GmbH,
D-26607 Aurich, Germany

E-Mail: ganna.papakina@stud.hshl.de
Web: www.hshl.de/

Abstract – The objective of this work was to develop a breast phantom with mechanical properties and radiation-absorption abilities comparable to female breast tissue, intended for validating an innovative mamma board. Two substances, polyvinylalcohol (PVAL) - hydrogel and silicone Ecoflex 0030, were examined for this purpose.
Initially, an underlying thorax phantom was constructed using CT images of a breast cancer patient. To create a compatible surface for various breast phantoms, the original breast was excised, and the phantom was produced using PLA in the large-format FDM 3D printer at the Hamm-Lippstadt University of Applied Sciences.
CAD was employed for designing breast models. For the initial tests, the breast model was generated using the RBSM Viewer software. [1] Upon successful construction, 3D scans of actual female patients' breasts were acquired and processed identically.
Molding was chosen as the manufacturing process of the breast phantoms due to the fluidity of the materials before curing. The molds were created utilizing the CAD models of the breasts and produced through an FDM 3D printer. The molds comprised two halves and a pouring opening, enabling the halves to be separated and the phantom to be extracted post-molding.
PVAL-hydrogel has been extensively studied for its ability to absorb radiation similarly to breast tissue, making it an ideal phantom in mammography. The gel is produced by continuously stirring PVAL powder in deionized water heated to at least 90°C until the powder particles fully dissolve. Afterward, the mixture must be cooled down by room temperature for two hours before it can be poured into the desired mold. Next, the mixture is subjected to a freeze-thaw cycle (FTC), involving freezing at -26°C for 12 hours followed by thawing at room temperature for several hours. Increasing the number of FTCs enhances the material stiffness. The concentrations that resemble breast tissue range from 5% to 20%, with the most pronounced similarity being at 10%. [2]
Testing included 10%, 7.5%, and 5% concentrations. An incomplete FTC was explored, creating a harder outer shell while maintaining inner flexibility at a 10% concentration. Challenges included uneven freezing, dehydration, and fragility.
The result indicates that the mold necessitates consistent wall thickness to facilitate the formation of a shell and prevent breakage when removing the phantom. However, freezing proved less effective on the thicker regions of the phantom. Furthermore, the phantom experienced dehydration and initiated decay within just a few days. Its moist surface posed challenges for attachment to the thorax phantom, and it proved fragile under mechanical loads, easily bursting and losing its inner fluid.
Ecoflex 0030 silicone, composed of parts A and B mixed in a 1A:1B ratio, was also tested. The silicone is utilized for imitating skin tissue in various applications, such as creating a prostate phantom, a surgical trainer, a mitral valve replica, an imitation of mammal skin, or even a soft robot mimicking human tongue. [3]–[7]

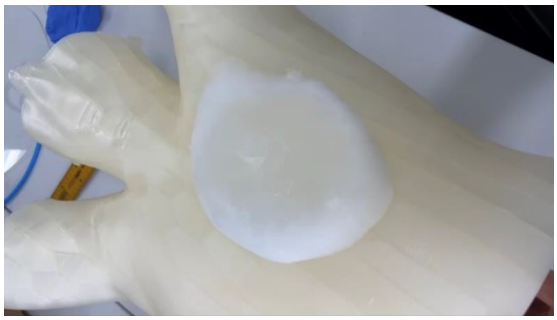

Fig.1: Hydrogel breast phantom prototype with 2x2-hour-FTCs. *Fig.2: Silicone breast phantom with the infill 94A: 6B*

After experimenting with the recommended ratio, the idea to vary the ratio of the components, similar to silicone gel implants, emerged. [8] The shell was produced using the prescribed ratio, while the infill was made using 94A: 6B. As a result, a phantom consisting of two halves, connected by a firm suture in the middle, was created.
The fabricated prototypes were subjected to ultrasound elastography to evaluate the modulus of elasticity and CT scanning to analyze the Hounsfield Unit (HU) values of the phantoms. For elastography, a range between 5 and 10 kPa was desired. The hydrogel prototype measured approximately 17 kPa and the silicone measured approximately 8 kPa. For the CT scans, the desired range is -150 HU to 50 HU. The hydrogel prototype had the closest HU values at approximately 23 HU. The silicon prototype was approximately 150 HU.
Comparing the two fabrication processes, the silicone breast phantom demonstrated advantages in both realistic motion behavior resembling breast tissue and durability compared to the hydrogel phantom, which had more similar Hounsfield unit values. In conclusion, the silicone fabrication has better potential overall, but the mold should be optimized to produce the phantom as a single unit.

References

[1] M. Weiherer, A. Eigenberger, B. Egger, V. Brébant, L. Prantl, and C. Palm, “Learning the shape of female breasts: an open-access 3D statistical shape model of the female breast built from 110 breast scans,” *Vis. Comput., Mar.* vol. 36, pp, 1597–1616, 2022, doi: 10.1007/s00371-022-02431-3.

[2] F. Oyiwoja Okoh, M. Fahmi Mohd Yusof, N. Ahmad Kabir, and S. Nor Azizah Abdullah, “Physical properties of polyvinyl alcohol (PVAL) gel materials as phantoms for mammography,” *IOP Conf. Ser. Mater. Sci. Eng.*, vol. 1231, no. 1, p. 012008, Feb. 2022, doi: 10.1088/1757-899X/1231/1/012008.

[3] T. Chiu, Z. Xiong, D. Parsons, M. R. Folkert, P. M. Medin, and B. Hrycushko, “Low-cost 3D print–based phantom fabrication to facilitate interstitial prostate brachytherapy training program,” *Brachytherapy*, vol. 19, no. 6, pp. 800–811, Nov. 2020, doi: 10.1016/j.brachy.2020.06.015.

[4] J. L. Sparks et al., “Use of silicone materials to simulate tissue biomechanics as related to deep tissue injury,” *Adv. Skin Wound Care*, vol. 28, no. 2, pp. 59–68, Feb. 2015, doi: 10.1097/01.ASW.0000460127.47415.6e.

[5] S. Engelhardt, S. Sauerzapf, B. Preim, M. Karck, I. Wolf, and R. De Simone, “Flexible and comprehensive patient-specific mitral valve silicone models with chordae tendineae made from 3D-printable molds,” *Int. J. Comput. Assist. Radiol. Surg.*, vol. 14, no. 7, pp. 1177–1186, Jul. 2019, doi: 10.1007/s11548-019-01971-9.

[6] P. Wei et al., “Flexible and stretchable electronic skin with high durability and shock resistance via embedded 3D printing technology for human activity monitoring and personal healthcare,” *Adv. Mater. Technol.*, vol. 4, no. 9, p. 1900315, 2019, doi: 10.1002/admt.201900315.

[7] X. Lu, W. Xu, and X. Li, “Concepts and simulations of a soft robot mimicking human tongue,” in 2015 6th International Conference on Automation, Robotics and Applications (ICARA), Feb. 2015, pp. 332–336. doi: 10.1109/ICARA.2015.7081169.

[8] M. A. Brook, “The chemistry and physical properties of biomedical silicones,” in W Peters et al. (Eds.) Biomaterials in Plastic Surgery, Woodhead Publishing, pp. 52–67, 2012. doi: 10.1533/9780857096418.52.

Organizing board

UNIVERSITÄT DUISBURG ESSEN

Westfälische Hochschule

FH AACHEN UNIVERSITY OF APPLIED SCIENCES

HOCHSCHULE HAMM-LIPPSTADT

Contact

info@yra-medtech.de
http://www.yra-medtech.de

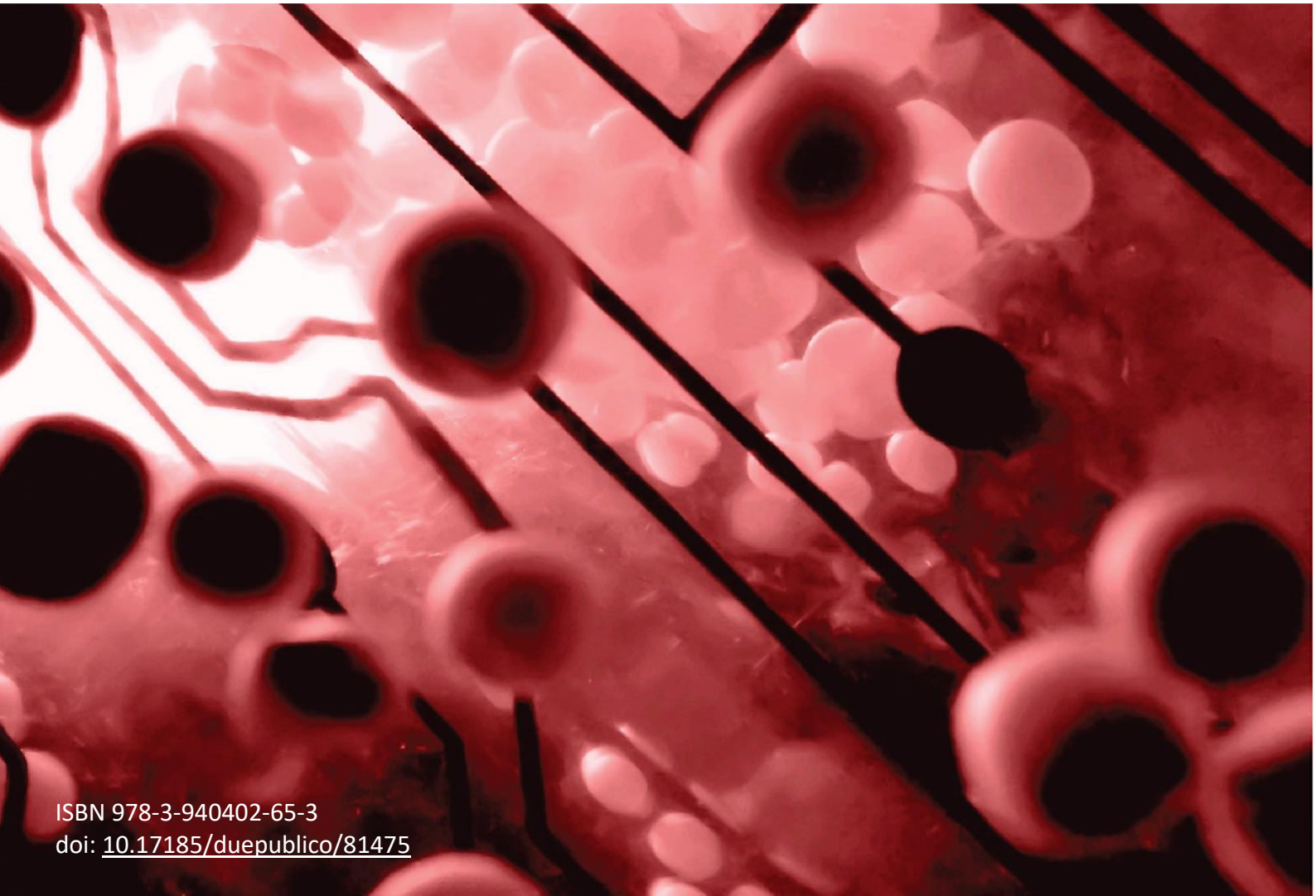

ISBN 978-3-940402-65-3
doi: 10.17185/duepublico/81475

DOI: 10.17185/duepublico/81475
URN: urn:nbn:de:hbz:465-20240125-152130-0